https://doi.org/10.5194/se-2020-64
Preprint. Discussion started: 5 May 2020

Solid Earth Discussions

Regional-scale paleofluid system across the Tuscan Nappe - Umbria Marche Arcuate Ridge (northern Apennines) as revealed by mesostructural and isotopic analyses of stylolite-vein networks

Nicolas Beaudoin[1,*], Aurélie Labeur[1,2], Olivier Lacombe[2], Daniel Koehn[3], Andrea Billi[4], Guilhem Hoareau[1], Adrian Boyce[5], Cédric M. John[7], Marta Marchegiano[7], Nick M. Roberts[6], Ian L. Millar[6], Fanny Claverie[8], Christophe Pecheyran[8], and Jean-Paul Callot[1].

1. Universite de Pau et des Pays de l'Adour, E2S UPPA, LFCR, Pau, France (nicolas.beaudoin@univ-pau.fr)
2. Sorbonne Université, CNRS-INSU, Institut des Sciences de la Terre de Paris - ISTeP, Paris, France
3. GeoZentrum Nordbayern, University Erlangen-Nuremberg, Erlangen, Germany
4. Consiglio Nationale delle Ricerche, Roma, Italy
5. Scottish Universities Environmental Research Centre (SUERC), East Killbride, UK
6. Geochronology and Tracers Facility, British Geological Survey, Environmental Science Centre, Nottingham, NG12 5GG, UK
7. Department of Earth Sciences & Engineering, Imperial College London, London, UK
8. Universite de Pau et des Pays de l'Adour, E2S UPPA, IPREM, Pau, France

Abstract

We report the results of a multi-proxy study that combines structural analysis of fracture-stylolite network and isotopic characterization of calcite vein cements/fault coating. Together with new paleopiezometric and radiometric constraints on burial evolution and deformation timing, these results provide a first-order picture of the regional fluid pathways network during the main stages of contraction in the Tuscan Nappe and Umbria Marche arcuate ridge (Northern Apennines).We reconstruct four continuous steps of deformation at the scale of the belt: burial that developed sedimentary stylolites, Apenninic-related layer parallel shortening with a contraction striking NE-SW, local extension related to folding, then a late stage of fold tightening under a contraction still striking NE-SW. In order to assess the timing and burial depth of strata at all stages, we combine a paleopiezometric tool based on inversion of the roughness of sedimentary stylolites that constrains the range of burial depth of strata prior to layer-parallel shortening, with burial models and U-Pb absolute dating of fault coatings. In the western part of the ridge, layer-parallel shortening started in Serravalian time (~12 Ma), then folding started at Tortonian time (~8 Ma), late stage fold tightening started in early Zanclean (~5 Ma) and likely lasted until recent/modern extension occurred (~3 Ma onward). This timing provides important constraints on the temperature that expectedly prevailed in the studied strata through its history. The textural and geochemical ($\delta^{18}O$, $\delta^{13}C$, $\Delta_{47}CO_2$ and $^{87}Sr/^{86}Sr$) study of calcite vein cements and fault coatings reveals that most of the fluids involved in the belt during deformation are local, or flowed laterally from the same reservoir. However, the western edge of the ridge recorded pulses of eastward squeegee-type migration of hydrothermal fluids (>140°C), that can be related to the difference in structural style of the subsurface between the eastern Tuscan Nappe and the Umbria Marche Ridge.

Introduction

The upper crust hosts ubiquitous fluid migrations that occur at all scales, leading to strain localization, earthquake triggering and georesource generation, distribution and storage (e.g., Cartwright, 2007;Andresen, 2012;Bjørlykke, 1994, 1993;Lacombe and Rolland, 2016;Lacombe et al.,

https://doi.org/10.5194/se-2020-64
Preprint. Discussion started: 5 May 2020

2014;Roure et al., 2005;Agosta et al., 2016). Since an important part of the world's exploited hydrocarbons, strategic ores and water resources are distributed in carbonate rocks (Agosta et al., 2010), it is fundamental to be able to properly depict the history of fluid migration in deformed rocks, not only to predict and monitor energy prospect and potential storage area, but also to understand which mechanisms make fluids migrate in carbonate rocks, what are the time and spatial scales of fluid flow involved, and what controls the diagenetic history of reservoirs.

Fluid migration events and related accumulations are usually linked to past tectonic events, especially to the fault/fracture pattern created during these tectonic events. Indeed, structural studies established that fracture networks in folded reservoirs are not exclusively related to the local folding history (Stearns and Friedman, 1972) and can also witness burial history (Becker et al., 2010;Laubach et al., 2010;Laubach et al., 2019) and long-term and large-scale regional deformation (Lacombe et al., 2011;Quintà and Tavani, 2012;Tavani and Cifelli, 2010;Tavani et al., 2015a;Bellahsen et al., 2006;Bergbauer and Pollard, 2004;Ahmadhadi et al., 2008;Sassi et al., 2012;Beaudoin et al., 2012). In fold-and-thrust belts and orogenic forelands, it is for instance possible to subdivide the mesoscale deformation (faults, veins, stylolites) history into specific stages: extension related to foreland flexure and bulging; pre-folding layer-parallel shortening (kinematically unrelated with folding); early folding layer-parallel shortening; syn-folding, strata curvature-related, local extension; late stage fold tightening, the last three stages being kinematically related with folding; and post folding contraction or extension (kinematically unrelated with folding). In the past decades, a significant volume of work has thus been conducted in order to reconstruct past fluid migrations through either localized fault systems or distributed sub-seismic fracture networks, in relationship with past tectonic events from the scale of a single fold to that of the basin itself (Engelder, 1984;Reynolds and Lister, 1987;McCaig, 1988;Evans et al., 2010;Forster and Evans, 1991;Cruset et al., 2018;Lacroix et al., 2011;Travé et al., 2000;Travé et al., 2007;Bjørlykke, 2010;Callot et al., 2017a;Callot et al., 2017b;Roure et al., 2010;Roure et al., 2005;Van Geet et al., 2002;Vandeginste et al., 2012;Vilasi et al., 2009;Barbier et al., 2012;Beaudoin et al., 2011;Beaudoin et al., 2014;Beaudoin et al., 2013). Studies highlighted that large-scale faults and sub-seismic scale fracture networks alike can impact the local fluid system, connecting compartments vertically and leading to local invasion of distant, hydrothermal fluids, over different time scales at the fold-scale (Beaudoin et al., 2011;Evans and Hobbs, 2003;Evans and Fischer, 2012;Barbier et al., 2012;Fischer et al., 2009;Lefticariu et al., 2005;Di Naccio et al., 2005). Fracture networks and related mineralizations can also be successfully used to describe the fluid system at the regional scale, with long term across-strike, stratigraphically-compartmentalized, fluid migration directed by compressive tectonic stress, with in some case an opening to external fluid flow, such as downward migration of meteoric fluids, or upward migration of hydrothermal fluids (*i.e.* hotter than the host-rock they precipitated in) of various origins (meteoric, marine, metamorphic), (Roure et al., 2005;Vandeginste et al., 2012;Cruset et al., 2018;Lacroix et al., 2011;Travé et al., 2000;Travé et al., 2007;De Graaf et al., 2019;Callot et al., 2010;Beaudoin et al., 2014;Bertotti et al., 2017;Gonzalez et al., 2013;Lucca et al., 2019;Mozafari et al., 2019;Storti et al., 2018;Vannucchi et al., 2010).

This contribution reports an orogen-scale paleofluid flow study in the Northern Apennine (Italy). The study builds upon the mesostructural and geochemical analysis of vein and stylolite networks within the competent Jurassic-Oligocene carbonate platform along a transect running across the Tuscan Nappe (TN) and the Umbria-Marche Apennines Ridge (UMAR) (Fig. 1a). The data collection was organized to cover a large area comprising several folds in order to be able to differentiate regional trends from local, fold-related ones. We focused on identifying and characterizing the first order

https://doi.org/10.5194/se-2020-64
Preprint. Discussion started: 5 May 2020

pattern of mesostructures – faults, fractures and stylolites – associated with LPS and with thrust-related folding, along with the stable isotope signatures ($\delta^{18}O$, $\delta^{13}C$), radiogenic signatures ($^{87}Sr/^{86}Sr$), clumped isotope signature ($\Delta_{47}CO_2$), and U-Pb absolute dating of their calcite cements. Without an appraisal of which fracture trends are relevant to the large scale (*i.e.*, regional) tectonic evolution, there was a risk to otherwise capture mesostructural and geochemical signals of local meaning only. In order to discuss the local versus hydrothermal fluid origin, we also considered burial curves derived from published dataset coupling sedimentary data and organic matter paleothermometers. Novel constraints are added to the timing and minimal depth of LPS-related deformation based on the study of the roughness properties of bedding-parallel stylolites, the inversion of which reliably returns the maximum depth at which compaction under a vertical maximum principal stress was still prevailing in the strata. U-Pb absolute dating of calcite steps on mesoscale faults further constrains the timing of folding. Such a multi-proxy approach, that combines structural analysis of fracture-stylolite network and isotopic characterization of cements, together with new constraints on burial evolution and deformation timing, provides for the first time a picture of the regional fluid pathways during the main stages of the Apenninic contraction.

1. Geological setting

The Neogene-to-Quaternary Apennines fold-and-thrust belt results from the convergence of Eurasia and Africa (Lavecchia, 1988;Elter et al., 2012). It is associated with the eastward retreating subduction of the Adriatic Plate under the European plate. The Apennines extend from the Po Plain to the Calabrian arc, and are divided into two main arcs, the Northern Apennines that extend down to the south of the UMAR, and the Southern Apennines that cover the remaining area down to the Calabrian arc (Carminati et al., 2010). The evolution of the Apennines is characterized by a roughly eastward migration of thrust fronts and associated foredeep basins, superimposed by post-orogenic extension at the rear of the eastward propagating orogenic belt (Cello et al., 1997;Tavani et al., 2012;Lavecchia, 1988;Ghisetti and Vezzani, 2002).

The study area, the Tuscan Nappe and the Umbria-Marches Apennines Ridge, comprises a succession of carbonate rocks, Late Triassic to Oligocene in age, which corresponds to a carbonate platform (Lavecchia, 1988;Carminati et al., 2010). The Umbrian carbonate units overlie early Triassic evaporites that act as a décollement level, itself unconformably overlying the crystalline basement rocks (Fig. 1b). Above the platform, Miocene turbidite deposits witness the progressive eastward involvement of the platform into the fold-and-thrust belt (Calamita et al., 1994). In the western part of the area, the belt is a thin-skinned assembly of piggy back duplex folds (Fig. 1c), the so-called Tuscan Nappe (TN), the folding and thrusting of which started by the Late Aquitanian and lasted until the Langhian (Carboni et al., 2020). The UMAR is an arcuate ridge exhibiting an eastward convexity, with a line connecting Perugia and Ancona separating a northern part where structural trends are oriented NW-SE, from a southern part where structure trends are oriented N-S (Calamita and Deiana, 1988). Burial models suggest that, from Burdigalian to early Messinian times, the TN was further buried under the allochthonous Ligurian thrust sheet, reaching locally up to 1 km in thickness (Caricchi et al., 2015). In the eastern part (now UMAR), the foreland was progressively folded and thrusted from the Lower Miocene in the westernmost part of the current ridge to the Messinian in the foreland of the ridge (Mazzoli et al., 2002). UMAR has been considered for long as a thin-skinned thrust belt where shortening was accommodated by stacking and duplexing of sedimentary units detached above a décollement level located in the Triassic evaporites (Conti and Gelmini, 1994;Carboni et al., 2020). The

https://doi.org/10.5194/se-2020-64
Preprint. Discussion started: 5 May 2020

seismic profile of the CROsta Profonda (CROP) project led authors to interpret the UMAR as resulting from thick-skinned tectonics, where the basement is involved in shortening (Barchi et al., 1998) through the positive inversion of normal faults inherited from the Jurassic Tethyan rifting (Fig. 1c). Even if the implication of the basement in shortening is seemingly more accepted now, the subsurface geometry is still debated, with some models involving shallow duplexes (Tavarnelli et al., 2004;Mirabella et al., 2008), while in more recent works surface folds are rather interpreted as related to high angle thrusts that either sole within the mid-Triassic décollement level, or involve the basement (Scisciani et al., 2014;Scisciani et al., 2019;Butler et al., 2004)(Fig. 1c). In these last views, the style of deformation of the UMAR strongly contrasts with the style of deformation of the TN where shortening is accommodated by allochtonous, far-travelled duplex nappes (Carboni et al., 2020)(Fig. 1c). The cross-section of Figure 1c also implies that at least part of the motion on the décollement level at the base of the TN postdates the westernmost activation of steep thrusts of the UMAR, as the thrust at the base of the TN cuts and offsets the west-verging basement fault in the area of Monte Subasio. Nowadays, the whole TN-UMAR area undergoes extension, with numerous active normal faults developing trenches, as the contraction front migrated toward the Adriatic Sea (d'Agostino et al., 2001).

Our sampling focused on the carbonate formations cropping out from W to E in the Cetona area located west from Perugia; the Monte Corona in the TN; the Monte Subasio, Gubbio Area, Spoletto Area, Monte Nero, Monte San Vicino, and Monte Cingoli in the UMAR, and the Monte Conero, the youngest onshore anticline related to the Apenninic compression, located on the coast line (Fig. 1a). The sampled units comprise, following the stratigraphic order (Fig. 1b): the Triassic anhydrites and dolostones of the Anidridi di Burano Formation with limestone and marl intercalation at the top; (2) Liassic massive dolomites of the Calcare Massiccio Fm. (Hettangian to Sinemurian); (3) the grey Jurassic limestones with chert beds of the Corniola Fm. (Lothangian-Pleisbachian); (4) the micritic limestones, marls, and cherts of the Bosso/Calcare Diasprini Fm (Toarcian-Tithonian); (5) the white limestones with chert beds of the Maiolica Fm. (Tithonian-Aptian); (6) the marly limestones of the Fucoidi Fm. (Aptian-Cenomanian); (7) the white marly limestones of the Scaglia Bianca Fm. (Cenomanian); (8) the pink marly limestones of the Scaglia Rossa Fm. (Turonian-Priabonian); and (9) the grey marly limestones of the Scaglia Cinera Fm. (Priabonian- Cattian). Up to 3000m of Miocene turbidites were deposited when the area of interest was the foredeep ahead of the advancing fold-and-thrust belt and during fold development, including clay-rich limestones and silts of Marnoso-Aranacea (Aquitanian-Tortonian); in the eastern part of the ridge (east from the Cingoli anticline), thicker foredeep deposits are Messinian to Pliocene in age.

2. Methods and results

We used structural and geochemical method to characterize the scenario of fluid rock interaction during deformation of the Umbria-Marche arcuate ridge in the Northern Apennines. Below, for each method, we explain the method itself and then we report the related results. We favour the presentation of the methods and related results in closed succession to make the latter as comprehensible as possible.

a. Mesostructural analysis of joints, veins and striated fault planes

i. Methodology

~1300 joint and vein orientations, along with tectonic stylolite orientations, were measured along a WSW-ENE transect going from Cetona in the TN to Monte Conero on the coastline (Fig. 1a). For each measurement site, fractures and tectonic stylolites (*i.e.* bedding perpendicular dissolution planes displaying horizontal peaks after unfolding or vertical dissolution planes displaying horizontal peaks in the current bed attitude) were measured. Chronological relationships were carefully observed in the field (Fig. 2) and checked in thin sections under the optical microscope when possible (Fig. 3). It is worthwhile noting that the veins of sets J1 and J2 show twinned calcite grains (Fig 3) with mostly thin and rectilinear twins (thickness < 5 μm)(Fig. 3). Poles to fractures and stylolite peaks were projected on Schmidt stereograms, lower hemisphere, in the current attitude of the strata (Raw), and after unfolding (Unfolded) as well (Fig. 4). Assuming the same mode of deformation (*i.e.* mode I opening joints/veins) and consistent chronological relationships and orientation, we use Fisher density to define statistically meaningful sets of joints. Tectonic stylolite planes and peaks were measured, and we consider that the average orientation of the stylolite peaks at the fold scale represents the orientation of the horizontal maximum principal stress σ1, as peaks grow parallel to the main shortening direction. To complement this mesostructural analysis, striated fault planes were measured (1) in the Langhian carbonates from the syncline West from San Vicino, and (2) in the forelimb of the Monte Subasio, with one site in the Scaglia Cinera and one site in the Scaglia Rossa e Bianca. At each site, paleostress orientations (local trend and plunge) and regimes were calculated using inversion techniques (Angelier, 1984). Published studies in the UMAR highlight the complexity of fracture patterns at the fold scale, that witness several phases of stress perturbation and stress/block rotation due to the local tectonics and structural inheritance(Tavani et al., 2008;Petracchini et al., 2012;Beaudoin et al., 2016;Díaz General et al., 2015). In order to capture the mesostructural and fluid flow evolution at the regional scale during layer-parallel shortening and folding, we gathered the most representative fracture data by structure, regardless of the structural complexity in the individual folds, and corrected them from the local bedding dip to discriminate between early and syn-folding features.

ii. Results

Based on the average orientation and the angle to the local fold axis, veins/joints can be gathered in 2 sets labelled J (Fig. 4): a first set J1 gathers joints/veins at high angle to bedding, that strike E-W to NE-SW but perpendicular to the local strike of fold axis. The trend of this set J1 evolves eastward as follows: E-W in the westernmost part (Cetona, Subasio), E-W to NE-SW in the central part (Catria, Nero), NE-SW in the eastern part of the chain (San Vicino, Cingoli), and ENE-WSW in the far foreland (Conero). The second set J2 gathers joints/veins at high angle to bedding that strike parallel to the local trend of the fold hinge, *i.e.* NW-SE in the ridge to N-S in the outermost part of the belt, where the arcuate shape is more marked. Note that as set J1 strikes perpendicular to the local strata direction, it is impossible to infer a pre-tilting or post-tilting (then called J3 hereinafter) origin for its development. In most case though, abutment relationships establish a relative chronology with set J1 predating set J2 (Fig. 3). Also, a third set comprising joints striking N-S while oblique to the direction of the fold axis is documented in the Monte Catria, but will not be considered further as it is not encountered elsewhere in the chain. Tectonic stylolites can be gathered as sets labelled S based on the orientation of their peaks. At first order, stylolites of which peaks are oriented NE-SW prevail : they are either bed-perpendicular, vertical with horizontal peaks in the unfolded attitude of strata, thus predating tilting (set S1), or ~vertical with ~horizontal peaks in the current attitude of strata, thus postdating tilting (set S2). However, because (1) stylolite data were often collected in shallow dipping

https://doi.org/10.5194/se-2020-64
Preprint. Discussion started: 5 May 2020

strata, (2) peaks are not always perpendicular to the stylolite planes and (3) the orientation data are scattered with intermediate plunges of the peaks, S1 and S2 are not always easily distinguished when both occurred. Another set showing stylolite planes with N-S peaks parallel to bedding, thus predating folding, is documented only at Monte Subasio, thus will not be integrated in the sequence at the scale of the fold-and-thrust belt. Finally, some mesoscale reverse and strike-slip conjugate fault systems have been measured (sets labelled F), of which fault-slip data inversion under specific assumptions (e.g., Lacombe, 2012) yields (1) a NE-SW contraction in the unfolded attitude of the strata (early folding set F1, bedding-parallel faults) and (2) a NE-SW contraction in the current attitude of the strata (late folding set F2, strike-slip conjugate faults and reverse faults).

b. Inversion of sedimentary stylolites

i. Methodology

Bedding-parallel stylolites are rough dissolution surfaces that developed in carbonates in flat laying strata during burial at the time when σ_1 was vertical. As proposed by Schmittbuhl et al. (2004) and later developed by Koehn et al. (2012), Ebner et al. (2009b);Ebner et al. (2010), Rolland et al. (2014) and Beaudoin et al. (2019);Beaudoin et al. (2020), the 1-D roughness of a track along the bedding-parallel stylolite (*i.e.* difference in height between two points along the track) results from a competition between roughening forces (*i.e.* pining on non-soluble particles in the rocks) and smoothening forces (*i.e.* the surface energy at scale typically < 1mm, and the elastic energy at scale > 1mm). The stylolite growth model (Koehn et al., 2007;Ebner et al., 2009a;Rolland et al., 2012;Toussaint et al., 2018) predicts that surface energy-controlled scale returns a steep slope characterized by a roughness exponent (so-called Hurst exponent) of 1.1, while the elastic energy-controlled scale returns a gentle slope with a roughness exponent of 0.6 (Fig. 5). The length at which the change in roughness exponent occurs, called the cross-over length (Lc, in mm), is directly related to the magnitude of differential and mean stress ($\sigma_d = \sigma_1 - \sigma_3$ and $\sigma_m = \frac{\sigma_1+\sigma_2+\sigma_3}{3}$, respectively, in Pa) prevailing in the strata at the time the stylolite stopped to be an active dissolution surface following:

$$Lc = \frac{\gamma E}{\beta \sigma_m \sigma_d} \qquad (1)$$

where E is the Young modulus of the rock (in Pa), γ is the solid-fluid interfacial energy (in J.m^{-2}), and β= ν(1-2ν)/π, a dimensionless constant with ν being the Poisson ratio. Samples of bedding parallel stylolites of which peaks were perpendicular to the dissolution plane were collected in specific points of the study area, and several stylolites were inverted. The inversion process follows the method described in Ebner et al. (2009b). Samples were cut perpendicular to the stylolite, hand polished to enhance the visibility of the track while being cautious about not altering the peaks, scanned at high-resolution (12800 pixel per inchs), and the 1D track was hand drawn with a pixel-based software (GIMP). Each track was analyzed as a periodic signal by using the Average Wavelet Spectrum with Daubechies D4 wavelets (Fig. 5) (Ebner et al., 2009b;Simonsen et al., 1998). In the case of bedding parallel stylolite related to compaction and burial, we assume the horizontal stress is isotropic in all direction ($\sigma_v >> \sigma_h = \sigma_H$) to simplify the equation 1 (Schmittbuhl et al., 2004) as:

$$\sigma_v^2 = \frac{\gamma E}{\alpha Lc} \qquad (2)$$

where $\alpha = \frac{(1-2\nu)*(1+\nu)^2}{30\pi(1-\nu)^2}$. According to the sampled formation, we used the solid-fluid interfacial energy γ of 0.24 J.m^{-2} for dolomite, and of 0.32 J.m^{-2} for calcite (Wright et al., 2001). As an

https://doi.org/10.5194/se-2020-64
Preprint. Discussion started: 5 May 2020

approximation for the material mechanical properties, we use a classic Poisson ratio of ν=0.25 ±0.05, and the average Young modulus derived from the Jurassic-Eocene competent core of E=24.2 GPa (Beaudoin et al., 2016). It is important to note that because of the non-linear regression method we use, and because of uncertainty on the mechanical parameters of the rock at the time it dissolved, the uncertainty on the stress has been calculated to be about 12% (Rolland et al., 2014). As the dissolution occurs along a fluidic film (Koehn et al., 2012;Rolland et al., 2012;Toussaint et al., 2018), the stylolite roughness is unaffected by local fluid overpressure until the system is fluidized and hydrofractures (Vass et al., 2014), meaning it is possible to translate vertical stress magnitude directly into depth if considering an average dry rock density for clastic/carbonated sediments (2400 $g.m^{-3}$, Manger (1963)), without any additional assumption on the past thermal gradient or fluid pressure (Beaudoin and Lacombe, 2018). This technique has already provided meaningful results in various settings (Bertotti et al., 2017;Rolland et al., 2014;Beaudoin et al., 2019;Beaudoin et al., 2020).

ii. Results

The paleopiezometric study of 30 bedding-parallel stylolites returned a range of burial depths, across the UMAR, from W to E, reported in table 1. Most data come from the western part of the UMAR: in the Subasio Anticline (n=7), the depth returned by the Scaglia Bianca and the lower part of the Scaglia Rossa Fms. ranges from ca. 800 ± 100 m to ca. 1450 ± 150 m. In Fiastra area (n=6), the depth returned for the Maiolica Fm. ranges from 800 ± 100 m to 1200 ± 150 m. In the Gubbio fault area (n=4), the depth returned for the Jurassic Corniola Fm. ranging from 600 ± 70 m to 1450 ± 150 m. In the Monte Nero (n=11), the depth data published by Beaudoin et al., (2016), and updated here range from 750 ± 100 m to 1350 ± 150 m in the Maiolica. Fewer data comes from the western part of the UMAR: in the Monte San Vicino (n=2), the depth returned for the Maiolica Fm. ranges from 1000 ± 100 m to 1050 ± 100 m. Finally, the depth reconstructed for the lower part of the Scaglia Rossa is 650 ± 70 m in the foreland at Conero Anticline (n=1).

c. Isotopic characterization of paleofluids (1) : O, C stable isotopes

i. Methodology

Calcite cements that filled up tectonic veins related either to layer-parallel shortening or to strata curvature at fold hinges were studied petrographically (Fig. 3). The vein textures were characterized in thin sections under an optical microscope, and diagenetic states were checked under cathodoluminescence, using a cathodoluminescence CITL CCL 8200 Mk4 operating under constant gun condition of 15kV and 300µA. To perform Oxygen and Carbon stable isotope analysis on the cements that were the most likely to witness the conditions of fluid precipitation at the time the veins opened, we selected those veins that (1) show no obvious evidence of shear; (2) the texture of which was elongated blocky or fibrous (Fig. 3); and (3) show homogeneous cement under cathodoluminescence (Fig. 3), precluding any posterior diagenetic alteration.

40 µg of calcite powder was hand sampled for each of 58 veins and 54 corresponding host-rocks in various structures and formation along the transect, in both TN and UMAR. Carbon and oxygen stable isotopes were analyzed at the Scottish Universities Environmental Research Centre (SUERC, East Kilbride, UK) on an Analytical Precision AP2003 mass spectrometer equipped with a separate acid injector system. As samples were either pure calcite or pure dolomite, we placed samples in glass vials to conduct a reaction with 105% H_3PO_4 under a helium atmosphere at 90°C. Results are reported in table 2, in permil relative to Vienna PeeDee Belemnite (‰ VPDB). Mean

https://doi.org/10.5194/se-2020-64
Preprint. Discussion started: 5 May 2020

analytical reproducibility based on replicates of the SUERC laboratory standard MAB-2 (Carrara Marble) was around ± 0.2‰ for both carbon and oxygen. MAB-2 is an internal standard extracted from the same Carrara Marble quarry, as is the IAEA-CO208 1 international standard. It is calibrated against IAEA-CO-1 and NBS-19.

ii. Results

At the scale of the study area, most formations cropping out were sampled (Table 2), and oxygen isotopic signatures of the vein cements and striated fault coatings range from -16.8‰ to 3.7‰ PDB while in the host rocks values range from -5.28 ‰ to 0.4‰ PDB. Carbon isotopic signatures range from -9.7‰ to 2.7‰ PDB, and from 0‰ to 3.5‰ PDB in the veins and in the host rock, respectively (Fig. 6a-b). Isotopic signatures are represented either according to the structure where they have been sampled, irrespective of the structural position in the structure (*i.e.* limbs or hinge), or according to the set they belong to, differentiating the sets J1, J2 and F1 (Fig. 6c). At the scale of the belt, isotopic signatures of host rocks are very similar, the only noteworthy point being that the Triassic carbonates are more depleted than the rest of the column ($\delta^{18}O$ of -5.5‰ to -3.5‰ versus -3.2‰ to -1‰ PDB). Considering the vein cements, an isotopic trend arises in the Jurassic-Eocene rocks with more depleted $\delta^{18}O$ values in or near the Tuscan nappe than in the UMAR (Fig. 6d), completely irrespective of the vein set, hence of the timing of opening. Especially, Monte Subasio and Monte Corona exhibit veins with very depleted $\delta^{18}O$ signatures < -15‰ PDB, while the most depleted $\delta^{18}O$ value in the UMAR is -7.3‰ PDB in the Monte San Vicino (Table 2). For the same dataset, the $\delta^{13}C$ values are rather similar in all structures and in all sets, a vast majority of veins showing cements with signatures of 1.5± 1.5‰ PDB.

d. Isotopic characterization of paleofluids (2): Sr radiogenic isotopes

i. Methodology

$^{87}Sr/^{86}Sr$ analysis was performed at the BGS in Keyworth (UK) with a VG Sector 54-30 multiple collector thermal ionization mass spectrometer. Mg-samples were loaded onto single Re filaments with a Ta-activator. An ^{88}Sr intensity of ~1 × 1011 A ± 10% was maintained. $^{87}Sr/^{86}Sr$ was corrected for mass fractionation to $^{86}Sr/^{88}Sr$ = 0.1194 after the exponential law described in Nier (1938). The 2 standard error internal precision on individual analyses ranges between 12 and 17 ppm (smaller than external reproducibility).

ii. Results

Analyses were carried out on 7 veins and 6 corresponding host rocks, spread on three structures of the UMAR (Monte Subasio, Monte Nero and Monte San Vicino, from the hinterland to the foreland) and three formations (the Calcare Massiccio, the Maiolica, and the Scaglia Fms., Fig. 7, Table 2). Vein sets sampled are the J1, J2 and J3 sets described in the whole area. Radiogenic signatures of host rocks spread in three different sets, one more radiogenic (Scaglia Rossa, $^{87}Sr/^{86}Sr$ ≈ 0.7078) a second one less radiogenic (Calcare Massicio, $^{87}Sr/^{86}Sr$ ≈0.7076), and a third one even less radiogenic (Scaglia Bianca and Calcare Rupestre $^{87}Sr/^{86}Sr$ ≈ 0.7073). Radiogenic signatures of host rocks are in line with expected values for seawater at the time of their respective deposition (McArthur et al., 2001). The radiogenic signatures of veins scatter from 0.7074 to 0.7077, with less radiogenic values in the Monte Nero and in the Monte San Vicino (sets J1, J2), and more radiogenic signatures in the Monte Subasio (Set J2). One vein cement of J3 in the Monte Subasio returned a lower radiogenic value of 0.7074.

e. Isotopic characterization of paleofluids (3): Carbonate clumped isotope paleothermometry (Δ_{47} CO_2)

i. Methodology

Clumped isotopes analyses were carried out in the Qatar Stable Isotope Laboratory at Imperial College London. The technique relies on the tendency for heavy isotopes (^{13}C, ^{18}O) to 'clump' together in the same carbonate molecule, that varies only by temperature. Since the clumping of heavy isotopes within a molecule is a purely stochastic process at high temperature but is systematically over-represented (relative to randomly distributing isotopes among molecules) at low temperature, the 'absolute' temperature of carbonate precipitation can be constrained using clumped isotope abundances.

Typical sample size was 3.5 mg of carbonate powder per replicate. Measurement of ^{13}C-^{18}O ordering in sample carbonate is achieved by measurement of the relative abundance of the $^{13}C^{18}O^{16}O$ isotopologues (mass 47) in acid evolved CO_2 and is referred in this paper as Δ_{47} CO_2. Samples were prepared on the automated clumped isotope measurement system (the IBEX: Imperial Batch Extraction system): the IBEX was developed at Imperial College London and is manufactured and distributed by Protiumms. A single run on the IBEX comprises 40 analysis, 30% of which are standards. Each analysis takes about 2 hours. The process starts with 10 minutes of reaction of the carbonate powder in a common acid bath containing 105% orthophosphoric acid at 90˚C to liberate CO_2. The CO_2 gas is then captured in a water/CO_2 trap maintained at liquid nitrogen temperature, and then moved through a hydrocarbon trap filled with poropak and a second water trap using helium as carrier gas. At the end of the cleaning process, the gas is transferred into a cold finger attached to the mass spectrometer, and into the bellows of the mass spectrometer. Following transfer, analyte CO_2 was measured on a dual inlet Thermo MAT 253 mass spectrometers (MS "Pinta"). The reference gas used is a high purity CO_2, with the following reference values: -37.07‰ $\delta^{13}C_{VPDB}$, 8.9‰ $\delta^{18}O_{VSMOW}$. Measurements comprise 8 acquisitions each with 7 cycles with 26s integration time. A typical acquisition time is 20 minutes, corresponding to a total analysis time of 2 hours.

Data processing was carried out in the freely available stable isotope management software, "Easotope" (John and Bowen, 2016) (www.easotope.org). The raw Δ_{47} CO_2 is corrected in three steps: mass spectrometer non-linearity was corrected by applying a "pressure baseline correction" (Bernasconi et al., 2013). Next, the Δ_{47} results were projected in the absolute reference frame or Carbon Dioxide Equilibrated Scale (CDES, Dennis et al. (2011)) based on routinely measured ETH1, ETH2, ETH3, ETH4 and Carrara Marble (ICM) carbonate standards (Meckler et al., 2014;Muller et al., 2017). The last correction to the raw Δ_{47} was to add an acid correction factor of 0.082‰ to obtain a final $\Delta_{47}CO_2$ value (Defliese et al., 2015). Temperatures of precipitation can then be estimated using the equation of Davies and John (2019). The bulk isotopic value of $\delta^{18}O$ is corrected for acid digestion at 90°C by multiplying the value by 1.0081 using the published fractionation factor (Kim et al., 2007). Contamination was monitored by observing the values on mass 48 and 49 from each measurement, using a Δ_{48} offset value > 0.5‰ and/or a 49 parameter values > 0.3 as a threshold to exclude individual replicates from the analysis (Davies and John, 2019).

ii. Results

13 samples were analyzed (Table 3), including cements of NE-SW (J1) and NW-SE (J2) pre-folding vein sets, along with coatings of early folding reverse (F1) and late folding strike-slip conjugate mesoscale faults (F2). Regardless of the structural position in the individual folds, veins were sampled

https://doi.org/10.5194/se-2020-64
Preprint. Discussion started: 5 May 2020

in the Monte Corona (TN), and in the UMAR at the Monte Subasio, the Monte San Vicino and the syncline to its west. Analysis of $\Delta_{47}CO_2$ returns the precipitation temperature (T) and the oxygen isotopic signature of the mineralizing fluid can be calculated using the $\delta^{18}O$ of the mineral, the clumped isotope temperature and the equation of Kim et al. (2007) (Fig. 8). Veins and faults belong to the Calcare Massiccio Fm., the Maiolica Fm., the Scaglia Fm., and the marls of the Langhian (Table 3). In the outermost structure studied (Monte Corona), the fractures of set J2 (n=2) return consistent precipitation temperatures T= 106 ± 8°C and $\delta^{18}O_{fluids}$ = 0 ± 1.8‰ VSMOW; the sample of the set J1 yields a T= 56 ± 16 °C and $\delta^{18}O_{fluids}$ = -1.1 ± 1.8‰ VSMOW; in the UMAR, at the Subasio anticline, set F1 (n=3) returns temperatures T ranging from 80±5°C to 141±19°C and a corresponding $\delta^{18}O_{fluids}$ ranging from 8.4±1‰ to 16.1±2.1‰ VSMOW, while the set J2 returns a T=71±0°C and $\delta^{18}O_{fluids}$ = -5.2±0‰ VSMOW; in the Monte Nero, set J1 (n=2) yields consistent T = 30±15°C and $\delta^{18}O_{fluids}$ =[2.7±2.4 to 6.8±0.2]‰ VSMOW; in the syncline on the west of the Monte San Vicino, set F2 (n=2) return T=[36±4 to 70±7]°C and $\delta^{18}O_{fluids}$ =[2.5±0.7 to 8.3±1.2]‰ VSMOW; in the Monte San Vicino, set J1 yields a T = 47 ± 5°C and $\delta^{18}O_{fluids}$ = 3.0±1.1‰ VSMOW while set J2 yields a T= 74± 10°C and $\delta^{18}O_{fluids}$ = 7.2±1.6‰ VSMOW.

f. U-Pb absolute dating of veins and faults

i. Methodology

The Calcite U-Pb geochronology was conducted in two different ways, of which specific methodology is reported as supplementary material:

- LA-ICPMS trace elements and U-Pb isotope mapping were performed at the Geochronology and Tracers Facility, British Geological Survey, UK, on 6 veins samples. Data were generated using a Nu Instruments Attom single collector inductively coupled plasma mass spectrometer coupled to a NWR193UC laser ablation system fitted with a TV2 cell, following protocol reported previously (Roberts et al., 2017;Roberts and Walker, 2016).

- LA-ICPMS U-Pb isotope mapping approach was undertaken at the Institut des Sciences Analytiques et de Physico-Chimie pour l'Environnement et les Matériaux (IPREM) Laboratory (Pau, France). All the 29 samples were analysed with a 257 nm femtosecond laser ablation system (Lambda3, Nexeya, Bordeaux, France) coupled to an HR-ICPMS Element XR (ThermoFisher Scientific, Bremen, Germany) fitted with the Jet Interface (Donard et al., 2015). The method is based on the construction of isotopic maps of the elements of interest for dating (U,Pb,Th) from ablation along lines, with ages calculated from the pixel values (Hoareau et al., 2020). The ablation was made in a helium atmosphere (600 mL min^{-1}), and 10 mL min^{-1} of nitrogen was added to the helium flow before mixing with argon in the ICPMS. Measured wash out time of the ablation cell was ~500 ms for helium gas. The fs-LA-ICP-MS coupling was tuned on a daily basis, and the additional Ar carrier gas flow rate, torch position and power were adjusted so that the U/Th ratio was close to 1 +/- 0.05 when ablating the glass SRM NIST612. Detector cross-calibration and mass bias calibration were checked daily. The laser and HR-ICPMS parameters used for U-Pb dating are detailed in the supplementary material.

ii. Results

Of the 35 samples screened for favorable U-Pb ratios, only 2 were selected for U-Pb dating (FAB5 and FAB6). Noteworthy, all samples from veins, whatever the set they belong to, reveal to have a U/Pb

https://doi.org/10.5194/se-2020-64
Preprint. Discussion started: 5 May 2020

Solid Earth Discussions

ratio not high enough to return an age, with a too low U content and/or dominated by common lead (see Supplementary material), which seems to be common in tectonic veins (Roberts et al., 2020). Only two samples consisting of calcite fault coating provided suitable material and were further analysed. Among these two, one could be successfully dated (FAB5). Despite a large majority of pixel values dominated by common lead with some scatter, the pixels with higher U/Pb ratios made it possible to obtain identical ages within the limits of uncertainty for the different plots (5.03 ± 1.2 Ma, 4.92 ± 1.3 Ma and 5.28 ± 0.95 Ma for the TW, the 86TW and the isochron plot, respectively) (Fig 9a). The rather large age uncertainties are consistent with the moderately high RSE values, but the d-MSWD values close to 1 indicate good alignment of discretized data (Fig. 9B). The other sample (FAB6) gave distinct ages according to the plot considered, ranging from 2.17 ± 1.4 Ma to 6.53 ± 2 Ma, due to low U/Pb ratios. Keeping in mind their low reliability, the ages obtained for this sample grossly point toward precipitation younger than ~8 Ma.

3. Interpretation of results and discussion

a. Sequence of fracturing events and related regional compressional and extensional trends

The previously defined joint/vein, fault and stylolite sets were compared and gathered in order to reconstruct the deformation history at the scale of the belt. We interpret the mesostructural network as witnessing three stages of regional deformation, supported by published fold-scale fracture sequence ((Tavani and Cifelli, 2010;Tavani et al., 2008;Petracchini et al., 2012;Beaudoin et al., 2016;Díaz General et al., 2015;Di Naccio et al., 2005;Vignaroli et al., 2013), in line with the ones observed in most recent studies (see Evans and Fischer, 2012; Tavani et al., 2015a for reviews) *:*

Layer parallel shortening (LPS) stage: chronological relationships statistically suggest that set J1 formed before set J2. Set J1 is kinematically consistent with set S1 that recorded the NE-SW Apenninic contraction, except in some places where sets J1 and S1 rather formed under a slight local rotation/perturbations of the NE-SW compression as a result of structural inheritance and/or of the arcuate shape of the fold. Bedding-parallel reverse faults of set F1 also belong to this LPS stage as they are likely to develop at an early stage of fold growth (Tavani et al., 2015a).

Folding stage: set J2 reflects local extension associated with strata curvature at fold hinges. The extensional trend, hence the trend of J2 joints/veins, changes as a function of curvature of fold axes in map view. We also interpret the stylolite peaks of which orientation are intermediate between set S1 and S2 (Fig. 4) as related to the folding stage (Roure et al., 2005).

Late stage fold tightening (LSFT): some stylolites with peaks striking NE-SW (set S2) and some veins/joints (set J3) postdate strata tilting and are consistent with late folding strike-slip and reverse faults (set F2). We gathered these sets as markers of a late stage of fold tightening (LSFT), *i.e*. with mesostructures still forming in response to contraction but slightly after fold growth ended.

It is noteworthy that the few occurrences of N-S striking veins/joints which are pre-folding and oblique to the fold axis (Fig. 4) could be tentatively related to a still earlier stage of *foreland flexure and bulging*, *i.e.* foredeep-parallel stretching associated with lithosphere flexuring (Tavani et al., 2013), even though the lithospheric forebulge was described only far east of the central Apennines area (Tavani et al., 2015b). However, these fractures, described in the Monte Nero (Beaudoin et al., 2016) and in

https://doi.org/10.5194/se-2020-64
Preprint. Discussion started: 5 May 2020

the Monte Catria (Tavani et al., 2008), were not interpreted by the authors because flexure/forebulge has never been recognized in the UMAR. We will not discuss these joints further.

b. Burial depth evolution and timing of contractional deformation

Stylolite roughness inversion applied to bedding-parallel stylolites (BPS) provides access to the maximum depth experienced by the strata at the time vertical shortening was prevailing on horizontal shortening, while σ_1 was vertical (Ebner et al., 2009b;Koehn et al., 2007;Beaudoin et al., 2019;Beaudoin et al., 2016;Beaudoin and Lacombe, 2018;Beaudoin et al., 2020;Rolland et al., 2014;Bertotti et al., 2017). In this study, we propose to compare the depth range returned by the inversion of a population of BPS to a local burial model (Fig. 10) reconstructed from the strata thickness documented in wells located in the western-central part of the UMAR (Nero-Catria area) (Centamore et al., 1979;Tavani et al., 2008). The timing of exhumation was constrained by published paleogeothermometric studies and by sedimentary records (Caricchi et al., 2014;Mazzoli et al., 2002). To the West, tectonic reconstructions and organic matter paleothermometry applied to the Tuscan Nappe (Caricchi et al., 2014) revealed that most of this unit underwent abnormal burial because it was underthrusted below the Ligurian Nappe, but that the western front of the Ligurian Nappe did not reach Monte Corona (Caricchi et al., 2014). We therefore consider a unique burial curve for the whole UMAR, and we project the range of depth values at which individual BPS stopped being active on the burial curves of the formations hosting the BPS. Recent application of this technique, coupled with absolute dating of vein cements (Beaudoin et al., 2018), showed that the greatest depth that a population of BPS recorded was reached nearly at the time corresponding to the age of the oldest LPS-related veins, suggesting that it is possible to constrain the timing at which horizontal principal stress overcame the vertical principal stress, switching from burial-related stress regime ($\sigma1$ vertical) to LPS ($\sigma1$ horizontal) (Beaudoin et al., 2020). In the case of the UMAR, this projection highlights that the BPS population started to stop being active at a depth as shallow as 800m in all studied formations, confirming that burial-related pressure solution (*i.e.*, chemical vertical compaction) initiated at even shallower depths (Ebner et al., 2009b;Rolland et al., 2014;Beaudoin et al., 2019;Beaudoin et al., 2020).

Figure 10 also shows that BPS were active mainly from the Cretaceous (age of deposition of the platform) until Serravallian times (~12 Ma), which suggests that LPS started around that time. As the sedimentary record pins the beginning of folding of the UMAR to the Tortonian in the west and to the Messinian in the east (onshore) (Calamita et al., 1994), we propose that, as an average, in the central and western part of the UMAR, the LPS stage of Apennine contraction lasted about ~4 Ma (Langhian to Tortonian) before folding occurred. Absolute dating of faults related to late stage fold tightening in the central part of the UMAR further indicates that fold development was over by the beginning of the Pliocene (~5 Ma). We can therefore estimate the duration of folding in the western-central part of the UMAR to ~3 Ma. Knowing the oldest record of post-orogenic extensional tectonics in the UMAR is mid-Pliocene (~3 Ma) (Barchi, 2010), we can also estimate the duration of the LSFT to ~2 Ma. In total, the period of time when the compressive horizontal principal stress $\sigma1$ was higher in magnitude that the vertical stress (*i.e.* until post-orogenic extension) lasted for 9 Ma in the Western-Central part of the UMAR. This 3 Ma can be considered as the average duration of the individual fold growth (~3 Ma), thus can be compared to the few attempts previously made to reconstruct the duration of fold growth. Using syntectonic sedimentation, various studies reconstructed constant fold growth lasting from between 3 to 10 Ma (Anastasio, 2007;Holl and Anastasio, 1993), up to 24 Ma with

https://doi.org/10.5194/se-2020-64
Preprint. Discussion started: 5 May 2020

quiescent periods in between growth pulses (Masaferro et al., 2002). From mechanical or kinematic modeling applied to natural cases, reconstructed folding duration range from 1 Ma to 8 Ma (Suppe et al., 1992;Yamato et al., 2011). The combination of bedding-parallel stylolite inversion, burial models and U-Pb dating of vein cements/fault coatings yields a valuable insight into the timing of the different stages of contraction in a fold-and-thrust belt (Beaudoin et al., 2018), quite in accordance with previous attempts to constrain fold growth duration and rates.

c. Paleofluid origin, precipitation temperature and pathways

i. Fluid system evolution

The combined use of BPS inversion and burial curves therefore constrains the absolute timing of LPS in the UMAR (Fig. 10). The further combination of the timing of LPS with the knowledge of the past geothermal gradient as reconstructed from organic matter studies in the eastern part of the TN (23°C/km, Caricchi et al., 2014) therefore yields the expected temperature within the various strata during the opening of the vein sets J1, J2 and J3, and faults F1 and F2. This makes it possible to identify potential fluids having precipitated in veins in thermal disequilibrium with the host rocks, e.g., of hydrothermal nature, during the Apenninic contraction, for all studied veins. The reconstructed temperatures of precipitation, and the maximum temperatures predicted by the burial model as well, are in agreement with the fact that most twins are thin (thickness < 5 μm) and rectilinear, suggesting deformation at temperature below 170°C (Ferrill et al., 2004;Lacombe, 2010). In spite of the Sr radiogenic signatures of the veins, that all fall into the range of expected values in the host rocks (Fig. 7) (McArthur et al., 2001), hinting for very limited exchange between reservoirs, geochemical datasets altogether discriminate two different fluid flow history at the belt scale: the folds at the TN-UMAR transition, *i.e.* Monte Corona and Monte Subasio, clearly exhibit a singular history compared to the other folds of the UMAR (Fig. 6d):

- in the UMAR, data suggest that during LPS, the fluid system mainly involved local fluids that mildly interacted with host rocks ($\delta^{18}O_{fluids} \approx 5‰$ VSMOW) and precipitated between 30°C and 50°C (Fig. 8), *i.e.*, at thermal equilibrium considering a depth of 1 to 1.7 km predicted at the time of LPS (Figs. 6, 10), and considering a surface temperature of 10°C and a geothermal gradient of 23°C/km (Caricchi et al., 2014). We interpret these fluids as local formational fluids (re)mobilized during pressure solution, burial and tectonic compaction and fracturing. During folding, fluid precipitation higher temperature (70°C) and higher degree of fluid rock interaction ($5< \delta^{18}O_{fluids} < 10‰$ VSMOW), are consistent with the expected temperature at the depth of burial of the Scaglia Fm. in the Tortonian (*i.e.*, at the time of folding), suggesting again a local source of fluids without significant migration at the reservoir scale (Fig. 6c-d). Previously published isotopic and thermometric data for contractional fluids flow in the easternmost part of the UMAR reported infill of hydrothermal (100°C) dolomitizing fluid flow during contraction (Mozafari et al., 2019;Storti et al., 2018). These hydrothermal dolomitizing fluids have the same range of signatures of $\delta^{18}O_{fluids}$ than the ones precipitating at the thermal equilibrium we document in the other folds of the UMAR (except monte Subasio). That suggests that the fluid system is rather local, with potential, local but seldom influence of faults to connect strata to deeper Jurassic reservoirs. During LSFT, the cement coating of faults F2 returns precipitation temperature of ca. 40°C to 70°C (Fig. 8), a temperature in line with the expected depth during the LSFT (Fig. 9).

- At the transition between the TN and the UMAR, Monte Subasio and Monte Corona both exhibit a similar fluid system evolution. During LPS, $\Delta_{47}CO_2$ and $\delta^{18}O$ signatures of vein cements and

https://doi.org/10.5194/se-2020-64
Preprint. Discussion started: 5 May 2020

Solid Earth Discussions
Open Access EGU

fault coating show a variability of temperature of precipitation and origin of fluids. Two different fluids can be defined (Fig. 6): (1) fluids precipitating at 50°C-70°C, *i.e.* at thermal equilibrium with the host rock, with $\delta^{18}O$ signatures of the fluids ranging from 0‰ to 5‰ SMOW, supporting a local formational marine source with no to small-scale migration, that precipitated has cements characterized by $\delta^{18}O$ between 0‰ and -10‰ PDB; (2) fluids that precipitated at 110°C to 140°C, *i.e.* hydrothermal, with very high $\delta^{18}O$ signatures of the fluids (up to 15‰ SMOW) that precipitated has cements characterized by very depleted $\delta^{18}O$ signatures (down to -17‰ PDB), and witnessing a migration of basinal brines, further supported by more radiogenic signatures of the $^{87}Sr/^{86}Sr$ ratios in Monte Subasio. During folding, we also document the hydrothermal fluids, but also fluids characterized by negative $\delta^{18}O_{fluids}$ that precipitated at a temperature consistent with predicted depth, interpreted as an input of meteoric water through fractures in the reservoir. Note that the hydrothermal dolomitizing fluids documented at the Montagna dei Fiori (Mozafari et al., 2019;Storti et al., 2018); have an isotopic signature much lower (6‰ SMOW) than the ones from the fluids involved in the Monte Subasio and Monte Corona (15‰ SMOW), supporting that a different fluid system was prevailing in this part of the belt during LPS, folding and LSFT.

ii. Fluid origin and engine of migration at the transition between the Tuscan Nappe and the Umbria-Marches Arcuate Ridge

During LPS and folding, the concomitant high temperatures of precipitation (>100°C) and the very positive O isotopic signatures of fluids ($\delta^{18}O_{fluids}$ > 10‰ VSMOW) indicate that the system was locally overprint either with formational-derived hydrothermal fluid migrating from depth > 4 km, or with hydrothermal Triassic fluids that have a very depleted original $\delta^{18}O_{fluids}$. Because the $^{87}Sr/^{86}Sr$ isotopic ratio is affected by neither fluid-rock interactions nor temperature changes, the radiogenic values of $^{87}Sr/^{86}Sr$ can help discriminate between both sources. In the present case, our data lead to discard the case where the fluids originated from Lower Triassic rocks and were remobilized during LPS. Indeed, expected $^{87}Sr/^{86}Sr$ values of lower Triassic seawater are significantly higher (0.7080-0.7082, (McArthur et al., 2001) than the $^{87}Sr/^{86}Sr$ values recorded by the fluids precipitating in the Monte Subasio (0.7076-0.07077) (Fig. 7). This range of radiogenic signature rather points out that the fluids were either formational fluids originating from the Scaglia rossa, that directly overlies the host rock, or local formational fluids that interacted with the clay fraction of the host-rocks. The coexistence inside a single deformation stage (LPS or folding) of both local/meteoric fluids and hydrothermal brines migrated from depths can be explained by transient flush into the system of hydrothermal fluids flowing from deeply buried part of the same, stratigraphically continuous, reservoir (Bachu, 1995;Garven, 1995;Machel and Cavell, 1999;Oliver, 1986).

We propose that the fluid system prevailing at the Monte Corona and at the Monte Subasio reflects an eastward, squeegee-type, flow of hydrothermal fluids (Fig. 11), for which the long-term migration engine is the lateral variation of the depth of the reservoir, buried under the stacked Tuscan and Ligurian Nappes in the west (up to 4 km, Caricchi et al., 2014), while just buried under the stratigraphic succession in the east (up to 2.5 km, Fig. 11b). This depth variation likely created a water table top difference in height, and so an hydraulic gradient allowing for the eastward fluid migration within the reservoir, enhanced by LPS and related fracture development (Roure et al., 2005). As the paleodepth variation was related to the weight of the nappes stacking rather than to a foreland-type slope, the UMAR would then have formed a plateau without any large-scale lateral fluid migrations

https://doi.org/10.5194/se-2020-64
Preprint. Discussion started: 5 May 2020

(Fig. 11b). The inferred pulses of hydrothermal fluids also implies a strong influence of forelandward propagation of contractional deformation in the eastward fluid expellation (Oliver, 1986;Machel and Cavell, 1999).

d. Influence of tectonic style on fluid flow during deformation history

Our study of the calcite cements that precipitated in tectonically controlled veins and faults at the scale of the UMAR and TN distinguishes two different fluid flow histories. East of Monte Subasio, *i.e.*, in the UMAR where shortening is distributed on deep-rooted faults, our data reveal a closed fluid system, with formational fluids precipitating at thermal equilibrium, limited fluid - host rock interactions in the reservoirs and limited cross-stratal fluid migration. In contrast, on the western part of this divide (in the TN), where shortening was accommodated by stacked nappes detached above the Triassic décollement level, high temperatures of fluids suggest the occurrence of eastward large-scale pulses of hydrothermal fluids (squeegee type, Fig. 11b).

If considering a thin-skinned tectonic model for the UMAR with shallow, low angle thrusts rooting on the Triassic evaporitic décollement level (Fig. 1) (Bally et al., 1986), one would expect some signature of Triassic fluids to be involved in the reservoir paleohydrology at the time faults were active or during folding, as illustrated in similar salt-detached fold systems in the Pyrenees, in the Appalachians, and in the Sierra Madre Oriental ((Lacroix et al., 2011;Travé et al., 2000;Evans and Hobbs, 2003;Evans and Fischer, 2012;Fischer et al., 2009;Smith et al., 2012;Lefticariu et al., 2005). One the other hand, if considering a thick-skinned tectonic model with high angle thrusts crossing the Triassic down to the basement, it becomes more likely that these thrusts did not act as efficient conduits for deep fluids (evaporitic fluids or basement fluids) as fault damage zones in evaporites remains non permeable, and if the displacement along the faults is smaller than the nonpermeable layer thickness. This contrasts with paleohydrological studies of basement cored folds, where high angle thrusts allow hot flashes of hydrothermal fluids into the overlying cover (Beaudoin et al., 2011;Evans and Fischer, 2012) in the absence of evaporites. Thus the lack of Triassic signature in our paleofluid dataset seems to support a thick-skinned tectonic style of deformation in the UMAR Fig. 11c).This fluid flow model therefore outlines important differences between belts where shortening is localized and accommodated by nappe stacking, typical from thin-skinned belts, and belts where shortening is instead distributed on several folds related to high angle thrusts, typical of thick-skinned belts (Lacombe and Bellahsen, 2016). Squeegee-type fluid flow during LPS in response to hydraulic gradient and lateral tectonic contraction has also been described in other thin-skinned belts, such as the Canadian Rocky Mountains (Vandeginste et al., 2012;Roure et al., 2010;Machel and Cavell, 1999;Qing and Mountjoy, 1992), or in Venezuela (Schneider et al., 2002;Schneider et al., 2004;Roure et al., 2003) where lithospheric bulging was the origin of the depth difference leading to hydraulic gradient-driven migrations. The presented case study shows how stacking of sedimentary units typical of thin-skinned tectonics strongly influences the fluid system beyond the morphological front of the belt, and can allow large scale fluid migrations even in the absence of (well-expressed) lithospheric forebulge occurred.

4. Conclusions

Our study of the vein-fault-tectonic stylolite populations distributed in Jurassic to Eocene limestone rocks at the scale of the thin-skinned Tuscan Nappe and presumably thick-skinned Umbria-

https://doi.org/10.5194/se-2020-64
Preprint. Discussion started: 5 May 2020

Marche Apenninic Ridge reveals the occurrence of several fracture/stylolite sets that support a three stages evolution of the Apenninic contraction : (1) layer-parallel shortening is reconstructed by a set of joint/veins striking NE-SW to E-W, perpendicular to the local trend of the fold, alongside with stylolite peaks striking NE-SW, and early folding bedding-parallel reverse faults; (2) folding stage is recorded by fold-parallel mode I joints and veins; (3) late stage fold tightening is recorded by late post-tilting, late folding stylolite peaks, joints/veins and also mesoscale reverse and strike-slip faults.

Thanks to burial models coupled to bedding-parallel stylolite paleopiezometry, along with (unfortunately scarce) U-Pb absolute dating of strike-slip faults related to late stage fold tightening, we were able to reconstruct the timing of the onset and the duration of the Apennine contraction, with an unparalleled detail: the LPS started by Langhian time (~12 Ma, inferred from the bedding parallel stylolite inversion), lasted for ~4 Ma, then folding started by the Tortonian time (8 Ma, from published syn-tectonic sedimentary constraints), lasted for ~3 Ma, LFST started by the beginning of Pliocene (5 Ma, given by absolute dating of fault coatings), itself lasting for 2 Ma before post-orogenic extension affected strata since mid-Pliocene (3 Ma).

Accessing the starting and ending timing of deformation in the UMAR also allowed us to predict the depth and expected temperatures of the paleofluid during fracturing assuming fluids precipitated at thermal equilibrium. By characterizing the cements related to sets of veins and faults using O and C stable isotope signatures, radiogenic signatures of $^{87/86}Sr$, and clumped isotopes of $\Delta^{47}CO_2$, we show that different paleofluid systems occurred during LPS and folding from west to east of the section. In the westernmost folds of the UMAR located beyond the arrow of the Ligurian Nappe thrusting over the Tuscan Nappe, we highlighted a local fluid system with transient flush of large-scale lateral, stratigraphically-compartimentalized migration of hydrothermal fluids. In contrast, these pulses are not documented in the rest of the UMAR and its foreland, where the fluid system remained closed at all time. We tentatively relate this change in fluid system to a lateral change in tectonic style of deformation across the belt, from thin-skinned in the TN to rather thick-skinned in the UMAR. Beyond regional implications, this study highlights the potential of such multi-proxy approach to unravel coupled structural and fluid flow evolution in fold-and-thrust belts.

Author contribution

NB, OL, DK, A. Billi, JPC were involved in the overall writing of the manuscript led by NB; NB, OL, DK, A. Billi collected structural data and rock samples in the field; NB, AL and OL conducted microstructural inversion; GH, A. Boyce, CJ, MM, NR, IM, FC and CP designed experiments and collected the geochemical data and wrote the related parts of the manuscript and appendices. All authors critically reviewed the multiple drafts of the manuscript.

5. Acknowledgments

This work has received funding from the Natural Environmental Research Council under grant number IP-1494-1114, from European Union's Seventh Framework Program for research, technological development, and demonstration under grant agreement 316889, and it also received funds from Sorbonne Université (research agreement C14313). NB is funded through the ISITE program E2S, supported by ANR PIA and Région Nouvelle-Aquitaine.

References

https://doi.org/10.5194/se-2020-64
Preprint. Discussion started: 5 May 2020

Agosta, F., Alessandroni, M., Antonellini, M., Tondi, E., and Giorgioni, M.: From fractures to flow: A field-based quantitative analysis of an outcropping carbonate reservoir, Tectonophysics, 490, 197-213, 10.1016/j.tecto.2010.05.005, 2010.

Agosta, F., Luetkemeyer, P. B., Lamarche, J., Crider, J. G., and Lacombe, O.: An introduction to the Special Issue: The role of fluids in faulting and fracturing in carbonates and other upper crustal rocks, Tectonophysics, 690, 1-3, 2016.

Ahmadhadi, F., Daniel, J. M., Azzizadeh, M., and Lacombe, O.: Evidence for pre-folding vein development in the Oligo-Miocene Asmari Formation in the Central Zagros Fold Belt, Iran, Tectonics, 27, 2008.

Anastasio, L.: Multiple scales of mechanical stratification and décollement fold kinematics, Sierra Madre Oriental foreland, northeast Mexico, Journal of Structural Geology, 29, 1241-1255, 2007.

Andresen, K. J.: Fluid flow features in hydrocarbon plumbing systems: What do they tell us about the basin evolution?, Marine Geology, 332, 89-108, 2012.

Angelier, J.: Tectonic analysis of fault slip data sets, Journal of Geophysical Research: Solid Earth, 89, 5835-5848, 1984.

Bachu, S.: Synthesis and model of formation-water flow, Alberta Basin, Canada, AAPG Bulletin, 79, 1159-1178, 1995.

Bally, A., Burbi, L., Cooper, C., and Ghelardoni, R.: Balanced cross sections and seismic reflection profiles across the central Apennines Mem, Soc. Geol. It., 35, 275-310, 1986.

Barbier, M., Hamon, Y., Callot, J.-P., Floquet, M., and Daniel, J.-M.: Sedimentary and diagenetic controls on the multiscale fracturing pattern of a carbonate reservoir: The Madison Formation (Sheep Mountain, Wyoming, USA), Marine and Petroleum Geology, 29, 50-67, 10.1016/j.marpetgeo.2011.08.009, 2012.

Barchi, M., De Feyter, A., Magnani, M., Minelli, G., Pialli, G., and Sotera, B.: Extensional tectonics in the Northern Apennines (Italy): evidence from the CROP03 deep seismic reflection line, Mem. Soc. Geol. It, 52, 527-538, 1998.

Barchi, M.: The Neogene–Quaternary evolution of the Northern Apennines: crustal structure, style of deformation and seismicity, Journal of Virtual Explorer, 36, 2010.

Beaudoin, N., Bellahsen, N., Lacombe, O., and Emmanuel, L.: Fracture-controlled paleohydrogeology in a basement-cored, fault-related fold: Sheep Mountain Anticline, Wyoming, United States, Geochemistry, Geophysics, Geosystems, 12, Q06011, 10.1029/2010gc003494, 2011.

Beaudoin, N., Leprêtre, R., Bellahsen, N., Lacombe, O., Amrouch, K., Callot, J.-P., Emmanuel, L., and Daniel, J.-M.: Structural and microstructural evolution of the Rattlesnake Mountain Anticline (Wyoming, USA): new insights into the Sevier and Laramide orogenic stress build-up in the Bighorn Basin, Tectonophysics, 576, 20-45, 2012.

Beaudoin, N., Lacombe, O., Bellahsen, N., and Emmanuel, L.: Contribution of studies of sub-seismic fracture populations to paleo-hydrological reconstructions (Bighorn Basin, USA), Procedia Earth and Planetary Science, 7, 57-60, 2013.

Beaudoin, N., Bellahsen, N., Lacombe, O., Emmanuel, L., and Pironon, J.: Crustal-scale fluid flow during the tectonic evolution of the Bighorn Basin (Wyoming, USA), Basin Research, 26, 403-435, 10.1111/bre.12032, 2014.

Beaudoin, N., Koehn, D., Lacombe, O., Lecouty, A., Billi, A., Aharonov, E., and Parlangeau, C.: Fingerprinting stress: Stylolite and calcite twinning paleopiezometry revealing the complexity of progressive stress patterns during folding-The case of the Monte Nero anticline in the Apennines, Italy, Tectonics, 35, 1687-1712, 10.1002/2016tc004128, 2016.

Beaudoin, N., and Lacombe, O.: Recent and future trends in paleopiezometry in the diagenetic domain: Insights into the tectonic paleostress and burial depth history of fold-and-thrust belts and sedimentary basins, Journal of Structural Geology, 114, 357-365, 10.1016/j.jsg.2018.04.001, 2018.

https://doi.org/10.5194/se-2020-64
Preprint. Discussion started: 5 May 2020

Beaudoin, N., Lacombe, O., Roberts, N. M. W., and Koehn, D.: U-Pb dating of calcite veins reveals complex stress evolution and thrust sequence in the Bighorn Basin, Wyoming, USA, Geology, 46, 1015-1018, 10.1130/g45379.1, 2018.

Beaudoin, N., Gasparrini, M., David, M.-E., Lacombe, O., and Koehn, D.: Bedding-parallel stylolites as a tool to unravel maximum burial depth in sedimentary basins: Application to Middle Jurassic carbonate reservoirs in the Paris basin, France, GSA Bulletin, 131, 1239-1254, 10.1130/b32064.1, 2019.

Beaudoin, N., Lacombe, O., Koehn, D., David, M.-E., Farrell, N., and Healy, D.: Vertical stress history and paleoburial in foreland basins unravelled by stylolite roughness paleopiezometry: Insights from bedding-parallel stylolites in the Bighorn Basin, Wyoming, USA, Journal of Structural Geology, 104061, 10.1016/j.jsg.2020.104061, 2020.

Becker, S., Eichhubl, P., Laubach, S. E., Reed, R. M., Lander, R., and Bodnar, R.: A 48 my history of fracture opening, temperature, and fluid pressure: Cretaceous Travis Peak Formation, East Texas basin, Bulletin, 122, 1081-1093, 2010.

Bellahsen, N., Fiore, P., and Pollard, D. D.: The role of fractures in the structural interpretation of Sheep Mountain Anticline, Wyoming, Journal of Structural Geology, 28, 850-867, 2006.

Bergbauer, S., and Pollard, D. D.: A new conceptual fold-fracture model including prefolding joints, based on the Emigrant Gap anticline, Wyoming, Geological Society of America Bulletin, 116, 294-307, 2004.

Bernasconi, S. M., Hu, B., Wacker, U., Fiebig, J., Breitenbach, S. F., and Rutz, T.: Background effects on Faraday collectors in gas-source mass spectrometry and implications for clumped isotope measurements, Rapid Communications in Mass Spectrometry, 27, 603-612, 2013.

Bertotti, G., de Graaf, S., Bisdom, K., Oskam, B., B. Vonhof, H., H. R. Bezerra, F., J. G. Reijmer, J., and L. Cazarin, C.: Fracturing and fluid-flow during post-rift subsidence in carbonates of the Jandaíra Formation, Potiguar Basin, NE Brazil, Basin Research, 29, 836-853, 10.1111/bre.12246, 2017.

Bjørlykke, K.: Fluid flow in sedimentary basins, Sedimentary Geology, 86, 137-158, 1993.

Bjørlykke, K.: Fluid-flow processes and diagenesis in sedimentary basins, Geological Society, London, Special Publications, 78, 127-140, 1994.

Bjørlykke, K.: Subsurface Water and Fluid Flow in Sedimentary Basins, in: Petroleum Geoscience, 259-279, 2010.

Butler, R. W. H., Mazzoli, S., Corrado, S., Donatis, M. D., Bucci, D. D., Gambini, R., Naso, G., Nicolai, C., Scrocca, D., Shiner, P., and Zucconi, V.: Applying Thick-skinned Tectonic Models to the Apennine Thrust Belt of Italy—Limitations and Implications. 2004.

Calamita, F., and Deiana, G.: The arcuate shape of the Umbria-Marche-Sabina Apennines (central Italy), Tectonophysics, 146, 139-147, 1988.

Calamita, F., Cello, G., Deiana, G., and Paltrinieri, W.: Structural styles, chronology rates of deformation, and time-space relationships in the Umbria-Marche thrust system (central Apennines, Italy), Tectonics, 13, 873-881, 1994.

Callot, J.-P., Breesch, L., Guilhaumou, N., Roure, F., Swennen, R., and Vilasi, N.: Paleo-fluids characterisation and fluid flow modelling along a regional transect in Northern United Arab Emirates (UAE), Arabian Journal of Geosciences, 3, 413-437, 2010.

Callot, J.-P., Roure, F., Faure, J.-L., and Tarapoanca, M.: Kinematic, thermal, and petroleum modeling of the northern Emirates, in: Petroleum System Analysis - Case Studies: AAPG Memoir, edited by: AbuAli, M. A., Moretti, I., and Nordgård Bolås, H. M., 135-164, 2017a.

Callot, J.-P., Sassi, W., Roure, F., Hill, K., Wilson, N., and Divies, R.: Pressure and Basin Modeling in Foothill Belts: A Study of the Kutubu Area, Papua New Guinea Fold and Thrust Belt, in: Petroleum Systems Analysis: AAPG Memoir, edited by: AbuAli, M. A., Moretti, I., and Nordgård Bolås, H. M., 165-190, 2017b.

Carboni, F., Brozzetti, F., Mirabella, F., Cruciani, F., Porreca, M., Ercoli, M., Back, S., and Barchi, M. R.: Geological and geophysical study of a thin-skinned tectonic wedge formed during an early collisional

https://doi.org/10.5194/se-2020-64
Preprint. Discussion started: 5 May 2020

stage: the Trasimeno Tectonic Wedge (Northern Apennines, Italy), Geological Magazine, 157, 213-232, 2020.

Caricchi, C., Aldega, L., and Corrado, S.: Reconstruction of maximum burial along the Northern Apennines thrust wedge (Italy) by indicators of thermal exposure and modeling, Geological Society of America Bulletin, 127, 428-442, 10.1130/b30947.1, 2014.

Caricchi, C., Aldega, L., and Corrado, S.: Reconstruction of maximum burial along the Northern Apennines thrust wedge (Italy) by indicators of thermal exposure and modeling, Bulletin, 127, 428-442, 2015.

Carminati, E., Lustrino, M., Cuffaro, M., and Doglioni, C.: Tectonics, magmatism and geodynamics of Italy: What we know and what we imagine, Journal of the Virtual Explorer, 36, 10.3809/jvirtex.2010.00226, 2010.

Cartwright, J.: The impact of 3D seismic data on the understanding of compaction, fluid flow and diagenesis in sedimentary basins, Journal of the Geological Society, 164, 881-893, 2007.

Cello, G., Mazzoli, S., Tondi, E., and Turco, E.: Active tectonics in the central Apennines and possible implications for seismic hazard analysis in peninsular Italy, Tectonophysics, 272, 43-68, 1997.

Centamore, E., Chiocchini, M., Chiocchini, U., Dramis, F., Giardini, G., Jacobacci, A., Martelli, G., Micarelli, A., and Potetti, M.: Carta Geologica d'Italia alla scala 1: 50.000. Note Illustrative F° 301 «Fabriano», 1979.

Conti, S., and Gelmini, R.: Miocene-Pliocene tectonic phases and migration of foredeep-thrust belt system in Northern Apennines, J Mem. Soc. Geol. It, 48, 261-274, 1994.

Cruset, D., Cantarero, I., Vergés, J., John, C. M., Muñoz-López, D., and Travé, A.: Changes in fluid regime in syn-orogenic sediments during the growth of the south Pyrenean fold and thrust belt, Global and Planetary Change, 171, 207-224, 10.1016/j.gloplacha.2017.11.001, 2018.

d'Agostino, N., Jackson, J., Dramis, F., and Funiciello, R.: Interactions between mantle upwelling, drainage evolution and active normal faulting: an example from the central Apennines (Italy), Geophysical Journal International, 147, 475-497, 2001.

Davies, A. J., and John, C. M.: The clumped (13C18O) isotope composition of echinoid calcite: Further evidence for "vital effects" in the clumped isotope proxy, Geochimica et Cosmochimica Acta, 245, 172-189, 2019.

De Graaf, S., Nooitgedacht, C. W., Le Goff, J., Van Der Lubbe, J. H., Vonhof, H. B., and Reijmer, J. J.: Fluid-flow evolution in the Albanide fold-thrust belt: Insights from hydrogen and oxygen isotope ratios of fluid inclusions, AAPG Bulletin, 103, 2421-2445, 2019.

Defliese, W. F., Hren, M. T., and Lohmann, K. C.: Compositional and temperature effects of phosphoric acid fractionation on Δ47 analysis and implications for discrepant calibrations, Chemical Geology, 396, 51-60, 2015.

Dennis, K. J., Affek, H. P., Passey, B. H., Schrag, D. P., and Eiler, J. M.: Defining an absolute reference frame for 'clumped'isotope studies of CO2, Geochemica Cosmochemica Acta, 75, 7117-7131, 2011.

Di Naccio, D., Boncio, P., Cirilli, S., Casaglia, F., Morettini, E., Lavecchia, G., and Brozzetti, F.: Role of mechanical stratigraphy on fracture development in carbonate reservoirs: Insights from outcropping shallow water carbonates in the Umbria–Marche Apennines, Italy, Journal of Volcanology and Geothermal Research, 148, 98-115, 2005.

Díaz General, E. N., Mollema, P. N., and Antonellini, M.: Fracture patterns and fault development in the pelagic limestones of the Monte Conero Anticline (Italy), Italian Journal of Geosciences, 134, 495-512, 2015.

Donard, A., Pottin, A.-C., Pointurier, F., and Pécheyran, C.: Determination of relative rare earth element distributions in very small quantities of uranium ore concentrates using femtosecond UV laser ablation–SF-ICP-MS coupling, Journal of Analytical Atomic Spectrometry, 30, 2420-2428, 2015.

Ebner, M., Koehn, D., Toussaint, R., and Renard, F.: The influence of rock heterogeneity on the scaling properties of simulated and natural stylolites, Journal of Structural Geology, 31, 72-82, 10.1016/j.jsg.2008.10.004, 2009a.

https://doi.org/10.5194/se-2020-64
Preprint. Discussion started: 5 May 2020

Ebner, M., Koehn, D., Toussaint, R., Renard, F., and Schmittbuhl, J.: Stress sensitivity of stylolite morphology, Earth and Planetary Science Letters, 277, 394-398, 10.1016/j.epsl.2008.11.001, 2009b.

Ebner, M., Piazolo, S., Renard, F., and Koehn, D.: Stylolite interfaces and surrounding matrix material: Nature and role of heterogeneities in roughness and microstructural development, Journal of Structural Geology, 32, 1070-1084, 10.1016/j.jsg.2010.06.014, 2010.

Elter, F. M., Elter, P., Eva, C., Eva, E., Kraus, R. K., Padovano, M., and Solarino, S.: An alternative model for the recent evolution of the Northern–Central Apennines (Italy), Journal of Geodynamics, 54, 55-63, 2012.

Engelder, T.: The role of pore water circulation during the deformation of foreland fold and thrust belts, Journal of Geophysical Research: Solid Earth, 89, 4319-4325, 1984.

Evans, M., and Hobbs, G.: Fate of ‘warm’migrating fluids in the central Appalachians during the Late Paleozoic Alleghanian orogeny, Journal of Geochemical Exploration, 78, 327-331, 2003.

Evans, M. A., Tollo, R., Bartholomew, M., Hibbard, J., and Karabinos, P.: Temporal and spatial changes in deformation conditions during the formation of the Central Appalachian fold-and-thrust belt: Evidence from joints, vein mineral paragenesis, and fluid inclusions, From Rodinia to Pangea: The Lithotectonic Record of the Appalachian Region, 206, 477, 2010.

Evans, M. A., and Fischer, M. P.: On the distribution of fluids in folds: A review of controlling factors and processes, Journal of Structural Geology, 44, 2-24, 2012.

Ferrill, D. A., Morris, A. P., Evans, M. A., Burkhard, M., Groshong Jr, R. H., and Onasch, C. M.: Calcite twin morphology: a low-temperature deformation geothermometer, Journal of structural Geology, 26, 1521-1529, 2004.

Fischer, M. P., Higuera-Díaz, I. C., Evans, M. A., Perry, E. C., and Lefticariu, L.: Fracture-controlled paleohydrology in a map-scale detachment fold: Insights from the analysis of fluid inclusions in calcite and quartz veins, Journal of Structural Geology, 31, 1490-1510, 2009.

Forster, C. B., and Evans, J. P.: Hydrogeology of thrust faults and crystalline thrust sheets: Results of combined field and modeling studies, Geophysical Research Letters, 18, 979-982, 1991.

Garven, G.: Continental-scale groundwater flow and geologic processes, Annual Review of Earth and Planetary Sciences, 23, 89-117, 1995.

Ghisetti, F., and Vezzani, L.: Normal faulting, extension and uplift in the outer thrust belt of the central Apennines (Italy): role of the Caramanico fault, Basin Research, 14, 225-236, 2002.

Gonzalez, E., Ferket, H., Callot, J.-P., Guilhaumou, N., Ortuno, F., and Roure, F.: Paleoburial, hydrocarbon generation and migration in the Cordoba platform and Veracruz basin: Insights from fluid inclusion studies and 2D-modelling, SEPM Special Publication, 103, 167 - 186, 2013.

Hoareau, G., Claverie, F., Pecheyran, C., Paroissin, C., Grignard, P. A., Motte, G., Chailan, O., and Girard, J. P.: Direct U-Pb dating of carbonates from micron scale fsLA-ICPMS images using robust regression, Geochronology Discuss., 2020, 1-23, 10.5194/gchron-2020-10, 2020.

Holl, J. E., and Anastasio, D. J.: Paleomagnetically derived folding rates, southern Pyrenees, Spain, Geology, 21, 271-274, 1993.

John, C. M., and Bowen, D.: Community software for challenging isotope analysis: First applications of ‘Easotope’to clumped isotopes, Rapid Communications in Mass Spectrometry, 30, 2285-2300, 2016.

Kim, S.-T., Mucci, A., and Taylor, B. E.: Phosphoric acid fractionation factors for calcite and aragonite between 25 and 75 C: revisited, Chemical Geology, 246, 135-146, 2007.

Koehn, D., Renard, F., Toussaint, R., and Passchier, C.: Growth of stylolite teeth patterns depending on normal stress and finite compaction, Earth and Planetary Science Letters, 257, 582-595, 10.1016/j.epsl.2007.03.015, 2007.

Koehn, D., Ebner, M., Renard, F., Toussaint, R., and Passchier, C. W.: Modelling of stylolite geometries and stress scaling, Earth and Planetary Science Letters, 341-344, 104-113, 10.1016/j.epsl.2012.04.046, 2012.

Lacombe, O.: Calcite twins, a tool for tectonic studies in thrust belts and stable orogenic forelands, Oil & Gas Science and Technology–Revue d’IFP Energies nouvelles, 65, 809-838, 2010.

https://doi.org/10.5194/se-2020-64
Preprint. Discussion started: 5 May 2020

Lacombe, O., Bellahsen, N., and Mouthereau, F.: Fracture patterns in the Zagros Simply Folded Belt (Fars, Iran): constraints on early collisional tectonic history and role of basement faults, Geological Magazine, 148, 940-963, 10.1017/s001675681100029x, 2011.
Lacombe, O.: Do fault slip data inversions actually yield “paleostresses” that can be compared with contemporary stresses? A critical discussion, Comptes Rendus Geoscience, 344, 159-173, 2012.
Lacombe, O., Swennen, R., and Caracausi, A.: An introduction to the Special Issue of Marine and Petroleum Geology: Fluid-rock-tectonics interactions in basins and orogens Introduction, Marine and Petroleum Geology, 55, 1-5, 2014.
Lacombe, O., and Bellahsen, N.: Thick-skinned tectonics and basement-involved fold–thrust belts: insights from selected Cenozoic orogens, Geological Magazine, 153, 763-810, 10.1017/s0016756816000078, 2016.
Lacombe, O., and Rolland, Y.: An introduction to the Special Issue: Fluids in crustal deformation: Fluid flow, fluid-rock interactions, rheology, melting and resources, Journal of Geodynamics, 101, 1-4, 2016.
Lacroix, B., Buatier, M., Labaume, P., Travé, A., Dubois, M., Charpentier, D., Ventalon, S., and Convert-Gaubier, D.: Microtectonic and geochemical characterization of thrusting in a foreland basin: Example of the South-Pyrenean orogenic wedge (Spain), Journal of Structural Geology, 33, 1359-1377, 10.1016/j.jsg.2011.06.006, 2011.
Laubach, S. E., Eichhubl, P., Hilgers, C., and Lander, R. H.: Structural diagenesis, Journal of Structural Geology, 32, 1866-1872, 10.1016/j.jsg.2010.10.001, 2010.
Laubach, S. E., Lander, R., Criscenti, L. J., Anovitz, L. M., Urai, J., Pollyea, R., Hooker, J. N., Narr, W., Evans, M. A., and Kerisit, S. N.: The role of chemistry in fracture pattern development and opportunities to advance interpretations of geological materials, Reviews of Geophysics, 57, 1065-1111, 2019.
Lavecchia, G.: The Tyrrhenian-Apennines system: structural setting and seismotectogenesis, Tectonophysics, 147, 263-296, 1988.
Lefticariu, L., Perry, E. C., Fischer, M. P., and Banner, J. L.: Evolution of fluid compartmentalization in a detachment fold complex, Geology, 33, 69-72, 2005.
Lucca, A., Storti, F., Balsamo, F., Clemenzi, L., Fondriest, M., Burgess, R., and Toro, G. d.: From Submarine to Subaerial Out-of-Sequence Thrusting and Gravity-Driven Extensional Faulting: Gran Sasso Massif, Central Apennines, Italy, tectonics, 38, 4155-4184, 10.1029/2019TC005783, 2019.
Machel, H. G., and Cavell, P. A.: Low-flux, tectonically-induced squeegee fluid flow, Bulletin of Canadian Petroleum Geology, 47, 510-533, 1999.
Manger, G. E.: Porosity and bulk density of sedimentary rocks, USGS Bulletin, 1144-E, 55, 1963.
Masaferro, J. L., Bulnes, M., Poblet, J., and Eberli, G. P.: Episodic folding inferred from syntectonic carbonate sedimentation: the Santaren anticline, Bahamas foreland, Sedimentary Geology, 146, 11-24, 2002.
Mazzoli, S., Deiana, G., Galdenzi, S., and Cello, G.: Miocene fault-controlled sedimentation and thrust propagation in the previously faulted external zones of the Umbria-Marche Apennines, Italy, EGU Stephan Mueller Special Publication Series, 1, 195-209, 2002.
McArthur, J. M., Howarth, R., and Bailey, T.: Strontium isotope stratigraphy: LOWESS version 3: best fit to the marine Sr-isotope curve for 0–509 Ma and accompanying look-up table for deriving numerical age, The Journal of Geology, 109, 155-170, 2001.
McCaig, A. M.: Deep fluid circulation in fault zones, Geology, 16, 867-870, 1988.
Meckler, A. N., Ziegler, M., Millán, M. I., Breitenbach, S. F., and Bernasconi, S. M.: Long-term performance of the Kiel carbonate device with a new correction scheme for clumped isotope measurements, Rapid Communications in Mass Spectrometry, 28, 1705-1715, 2014.
Mirabella, F., Barchi, M., Lupattelli, A., Stucchi, E., and Ciaccio, M.: Insights on the seismogenic layer thickness from the upper crust structure of the Umbria-Marche Apennines (central Italy), Tectonics, 27, TC1010, 2008.

https://doi.org/10.5194/se-2020-64
Preprint. Discussion started: 5 May 2020

Solid Earth Discussions

Mozafari, M., Swennen, R., Balsamo, F., Desouky, H. E., Storti, F., and Taberner, C.: Fault-controlled dolomitization in the Montagna dei Fiori Anticline (Central Apennines, Italy): record of a dominantly pre-orogenic fluid migration, solid earth, 10, 1355-1383, 10.5194/SE-10-1355-2019, 2019.

Muller, I. A., Violay, M. E. S., Storck, J. C., Fernandez, A., van Dijk, J., Madonna, C., and Bernasconi, S. M.: Clumped isotope fractionation during phosphoric acid digestion of carbonates at 70 degrees C, Chemical Geology, 449, 1-14, 10.1016/j.chemgeo.2016.11.030, 2017.

Nier, A. O.: The isotopic constitution of strontium, barium, bismuth, thallium and mercury, Physical Review, 54, 275, 1938.

Oliver, J.: Fluids expelled tectonically from orogenic belts: Their role in hydrocarbon migration and other geologic phenomena, Geology, 14, 99-102, 1986.

Petracchini, L., Antonellini, M., Billi, A., and Scrocca, D.: Fault development through fractured pelagic carbonates of the Cingoli anticline, Italy: Possible analog for subsurface fluid-conductive fractures, Journal of Structural Geology, 45, 21-37, 10.1016/j.jsg.2012.05.007, 2012.

Qing, H., and Mountjoy, E.: Large-scale fluid flow in the Middle Devonian Presqu'ile Barrier, Western Canada sedimentary basin, Geology, 20, 903-906, 1992.

Quintà, A., and Tavani, S.: The foreland deformation in the south-western Basque–Cantabrian Belt (Spain), Tectonophysics, 576, 4-19, 2012.

Reynolds, S. J., and Lister, G. S.: Structural aspects of fluid-rock interactions in detachment zones, Geology, 15, 362-366, 1987.

Roberts, N. M., and Walker, R. J.: U-Pb geochronology of calcite-mineralized faults: Absolute timing of rift-related fault events on the northeast Atlantic margin, Geology, 44, 531-534, 2016.

Roberts, N. M., Rasbury, E. T., Parrish, R. R., Smith, C. J., Horstwood, M. S., and Condon, D. J.: A calcite reference material for LA-ICP-MS U-Pb geochronology, Geochem Geophys Geosyst, 18, 2807-2814, 2017.

Roberts, N. M. W., Drost, K., Horstwood, M. S. A., Condon, D. J., Chew, D., Drake, H., Milodowski, A. E., McLean, N. M., Smye, A. J., Walker, R. J., Haslam, R., Hodson, K., Imber, J., Beaudoin, N., and Lee, J. K.: Laser ablation inductively coupled plasma mass spectrometry (LA-ICP-MS) U–Pb carbonate geochronology: strategies, progress, and limitations, Geochronology, 2, 33-61, 10.5194/gchron-2-33-2020, 2020.

Rolland, A., Toussaint, R., Baud, P., Schmittbuhl, J., Conil, N., Koehn, D., Renard, F., and Gratier, J.-P.: Modeling the growth of stylolites in sedimentary rocks, Journal of Geophysical Research: Solid Earth, 117, B06403, 10.1029/2011jb009065, 2012.

Rolland, A., Toussaint, R., Baud, P., Conil, N., and Landrein, P.: Morphological analysis of stylolites for paleostress estimation in limestones, International Journal of Rock Mechanics and Mining Sciences, 67, 212-225, 10.1016/j.ijrmms.2013.08.021, 2014.

Roure, F., Bordas-Lefloch, N., Toro, J., Aubourg, C., Guilhaumou, N., Hernandez, E., Lecornec-Lance, S., Rivero, C., Robion, P., and Sassi, W.: Petroleum systems and reservoir appraisal in the sub-Andean basins (eastern Venezuela and eastern Colombian foothills), AAPG Memoirs, 79, 750-775, 2003.

Roure, F., Swennen, R., Schneider, F., Faure, J., Ferket, H., Guilhaumou, N., Osadetz, K., Robion, P., and Vandeginste, V.: Incidence and importance of tectonics and natural fluid migration on reservoir evolution in foreland fold-and-thrust belts, Oil & Gas Science and Technology, 60, 67-106, 2005.

Roure, F., Andriessen, P., Callot, J.-P., Faure, J.-L., Ferket, H., Gonzales, E., Guilhaumou, N., Lacombe, O., Malandain, J., and Sassi, W.: The use of palaeo-thermo-barometers and coupled thermal, fluid flow and pore-fluid pressure modelling for hydrocarbon and reservoir prediction in fold and thrust belts, Geological Society, London, Special Publications, 348, 87-114, 2010.

Sassi, W., Guiton, M., Leroy, Y., Daniel, J.-M., and Callot, J.-P.: Constraints on bed scale fracture chronology with a FEM mechanical model of folding: The case of Split Mountain (Utah, USA), Tectonophysics, 576, 197-215, 2012.

Schmittbuhl, J., Renard, F., Gratier, J. P., and Toussaint, R.: Roughness of stylolites: implications of 3D high resolution topography measurements, Phys Rev Lett, 93, 238501, 10.1103/PhysRevLett.93.238501, 2004.

https://doi.org/10.5194/se-2020-64
Preprint. Discussion started: 5 May 2020

Solid Earth Discussions

Schneider, F., Faure, J., and Roure, F.: Methodology for basin modeling in complex area: examples from Eastern Venezuelan and Canadian Foothills, AAPG Hedberg Conference “Deformation History, Fluid Flow Reconstruction and Reservoir Appraisal in Foreland Fold and Thrust Belts 2002, 14-18,

Schneider, F., Pagel, M., and Hernandez, E.: Basin modeling in a complex area: Example from the Eastern Venezuelan foothills, in: Deformation, fluid flow, and reservoir appraisal in foreland fold and thrust belts: AAPG Hedberg Series, edited by: Swennen, R., Roure, F., and Granath, J. W., 357-369, 2004.

Scisciani, V., Agostini, S., Calamita, F., Pace, P., Cilli, A., Giori, I., and Paltrinieri, W.: Positive inversion tectonics in foreland fold-and-thrust belts: a reappraisal of the Umbria–Marche Northern Apennines (Central Italy) by integrating geological and geophysical data, Tectonophysics, 637, 218-237, 2014.

Scisciani, V., Patruno, S., Tavarnelli, E., Calamita, F., Pace, P., and Iacopini, D.: Multi-phase reactivations and inversions of Paleozoic–Mesozoic extensional basins during the Wilson cycle: case studies from the North Sea (UK) and the Northern Apennines (Italy), Geological Society, London, Special Publications, 470, 205-243, 10.1144/sp470-2017-232, 2019.

Simonsen, I., Hansen, A., and Nes, O. M.: Determination of the Hurst exponent by use of wavelet transforms, Physical Review E, 58, 2779, 1998.

Smith, A. P., Fischer, M. P., and Evans, M. A.: Fracture-controlled palaeohydrology of a secondary salt weld, La Popa Basin, NE Mexico, Geological Society, London, Special Publications, 363, 107-130, 2012.

Stearns, D. W., and Friedman, M.: Reservoirs in fractured rock: Geologic exploration methods, 1972.

Storti, F., Balsamo, F., Mozafari, M., Koopman, A., Swennen, R., and Taberner, C.: Syn-Contractional Overprinting Between Extension and Shortening Along the Montagna Dei Fiori Fault During Plio-Pleistocene Antiformal Stacking at the Central Apennines Thrust Wedge Toe, Tectonics, 37, 3690-3720, 10.1029/2018tc005072, 2018.

Suppe, J., Chou, G. T., and Hook, S. C.: Rates of folding and faulting determined from growth strata, in: Thrust tectonics, Springer, 105-121, 1992.

Tavani, S., Storti, F., Salvini, F., and Toscano, C.: Stratigraphic versus structural control on the deformation pattern associated with the evolution of the Mt. Catria anticline, Italy, Journal of Structural Geology, 30, 664-681, 10.1016/j.jsg.2008.01.011, 2008.

Tavani, S., and Cifelli, F.: Deformation pattern analysis and tectonic implications of a décollement level within the Central Apennines (Italy), Geological Journal, 45, 582-596, 10.1002/gj.1198, 2010.

Tavani, S., Storti, F., Bausà, J., and Muñoz, J. A.: Late thrusting extensional collapse at the mountain front of the northern Apennines (Italy), Tectonics, 31, TC4019, 10.1029/2011tc003059, 2012.

Tavani, S., Iannace, A., Mazzoli, S., Vitale, S., and Parente, M.: Late Cretaceous extensional tectonics in Adria: Insights from soft-sediment deformation in the Sorrento Peninsula (southern Apennines), Journal of Geodynamics, 68, 49-59, 10.1016/j.jog.2013.03.005, 2013.

Tavani, S., Storti, F., Lacombe, O., Corradetti, A., Muñoz, J., and Mazzoli, S.: A review of deformation pattern templates in foreland basin systems and fold-and-thrust belts: Implications for the state of stress in the frontal regions of thrust wedges, Earth-Science Reviews, 141, 82-104, 2015a.

Tavani, S., Vignaroli, G., and Parente, M.: Transverse versus longitudinal extension in the foredeep-peripheral bulge system: Role of Cretaceous structural inheritances during early Miocene extensional faulting in inner central Apennines belt, Tectonics, 34, 1412-1430, 2015b.

Tavarnelli, E., Butler, R., Decandia, F., Calamita, F., Grasso, M., Alvarez, W., Renda, P., Crescenti, U., and D’offizi, S.: Implications of fault reactivation and structural inheritance in the Cenozoic tectonic evolution of Italy, The Geology of Italy, Special, 1, 209-222, 2004.

Toussaint, R., Aharonov, E., Koehn, D., Gratier, J. P., Ebner, M., Baud, P., Rolland, A., and Renard, F.: Stylolites: A review, Journal of Structural Geology, 114, 163-195, 10.1016/j.jsg.2018.05.003, 2018.

Travé, A., Calvet, F., Sans, M., Vergés, J., and Thirlwall, M.: Fluid history related to the Alpine compression at the margin of the south-Pyrenean Foreland basin: the El Guix anticline, Tectonophysics, 321, 73-102, 2000.

Travé, A., Labaume, P., and Vergés, J.: Fluid systems in foreland fold-and-thrust belts: an overview from the Southern Pyrenees, in: Thrust belts and foreland basins, Springer, 93-115, 2007.

https://doi.org/10.5194/se-2020-64
Preprint. Discussion started: 5 May 2020

Solid Earth
Discussions
Open Access

Van Geet, M., Swennen, R., Durmishi, C., Roure, F., and Muchez, P.: Paragenesis of Cretaceous to Eocene carbonate reservoirs in the Ionian fold and thrust belt (Albania): relation between tectonism and fluid flow, Sedimentology, 49, 697-718, 2002.

Vandeginste, V., Swennen, R., Allaeys, M., Ellam, R. M., Osadetz, K., and Roure, F.: Challenges of structural diagenesis in foreland fold-and-thrust belts: a case study on paleofluid flow in the Canadian Rocky Mountains West of Calgary, Marine and Petroleum Geology, 35, 235-251, 2012.

Vannucchi, P., Remitti, F., Bettelli, G., Boschi, C., and Dallai, L.: Fluid history related to the early Eocene-middle Miocene convergent system of the Northern Apennines (Italy): Constraints from structural and isotopic studies, journal of geophysical research, 115, 10.1029/2009JB006590, 2010.

Vass, A., Koehn, D., Toussaint, R., Ghani, I., and Piazolo, S.: The importance of fracture-healing on the deformation of fluid-filled layered systems, Journal of Structural Geology, 67, 94-106, 10.1016/j.jsg.2014.07.007, 2014.

Vignaroli, G., Pinton, A., De Benedetti, A. A., Giordano, G., Rossetti, F., Soligo, M., and Berardi, G.: Structural compartmentalisation of a geothermal system, the Torre Alfina field (central Italy), Tectonophysics, 608, 482-498, 2013.

Vilasi, N., Malandain, J., Barrier, L., Callot, J.-P., Amrouch, K., Guilhaumou, N., Lacombe, O., Muska, K., Roure, F., and Swennen, R.: From outcrop and petrographic studies to basin-scale fluid flow modelling: The use of the Albanian natural laboratory for carbonate reservoir characterisation, Tectonophysics, 474, 367-392, 2009.

Wright, K., Cygan, R. T., and Slater, B.: Structure of the (101 [combining macron] 4) surfaces of calcite, dolomite and magnesite under wet and dry conditions, Physical Chemistry Chemical Physics, 3, 839-844, 2001.

Yamato, P., Kaus, B. J., Mouthereau, F., and Castelltort, S.: Dynamic constraints on the crustal-scale rheology of the Zagros fold belt, Iran, Geology, 39, 815-818, 2011.

Figures with captions

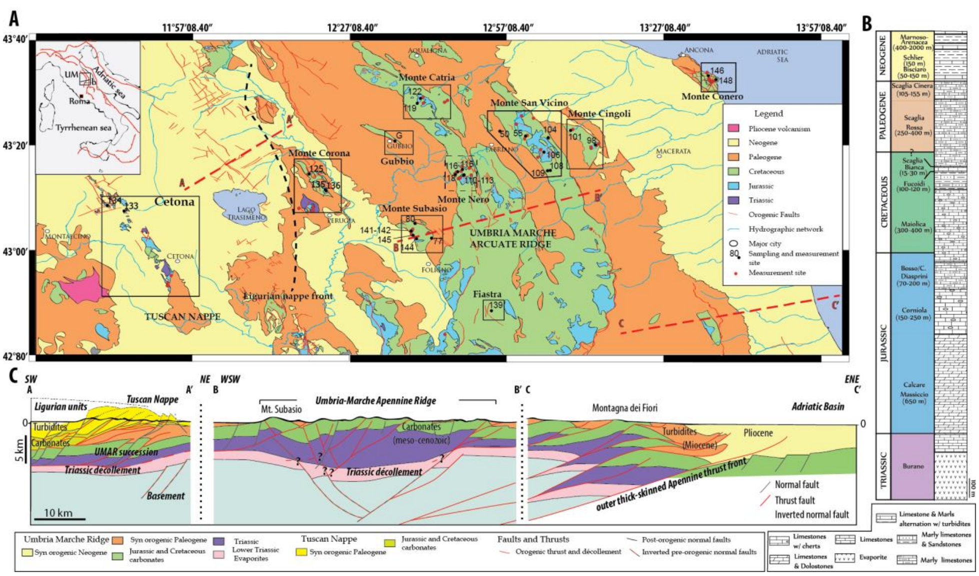

Figure 1: Simplified geological map of the study area, with located the sampling and measurement sites. Frames relate to the fracture study areas used in figure 4. Exact location of measurement sites are reported as black and red points, and labelled black points also represent the sampling site for geochemical analysis. B. Stratigraphic column based on stratigraphic and well data from the central

https://doi.org/10.5194/se-2020-64
Preprint. Discussion started: 5 May 2020

part of the UMAR, after Centamore et al. (1979). C. Crustal-scale composite cross-section based on published seismic data interpretations, A-A' modified after Carboni et al. (2020); B-B' and C-C' after Scisciani et al. (2014). Note that both tectonic style (thick-skinned and thin-skinned) are represented by question marks for the UMAR.

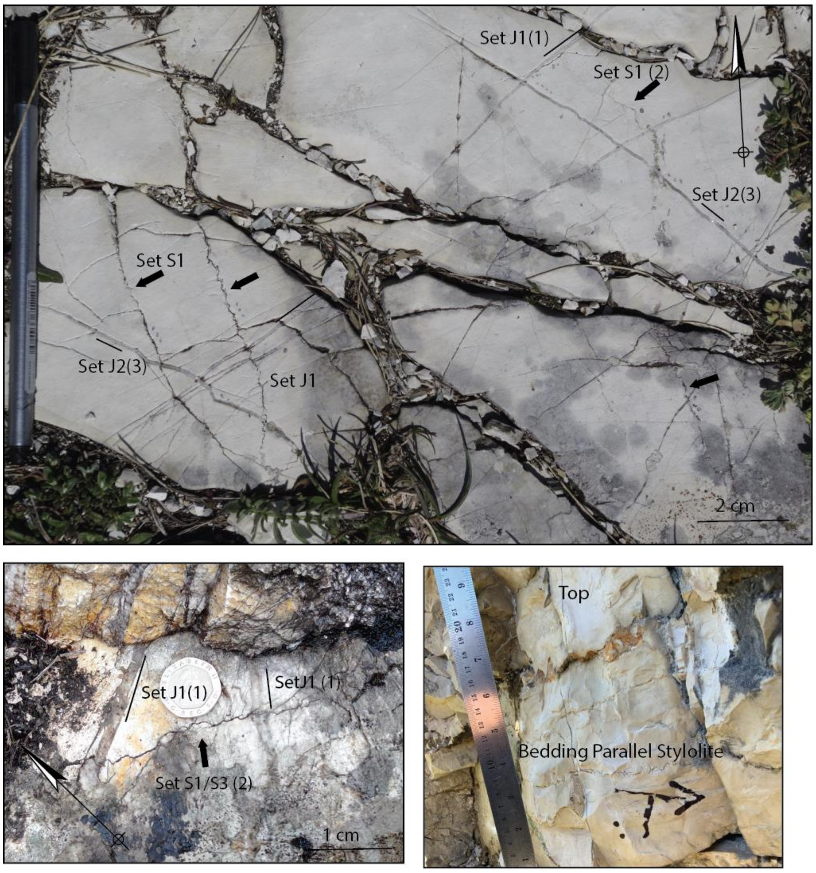

Figure 2: Field photographs showing chronological relationships between veins/joints and stylolites. A) Monte Nero, b) Monte Cingoli, c) Monte Subasio. Sets are reported along with local chronological order between brackets.

https://doi.org/10.5194/se-2020-64
Preprint. Discussion started: 5 May 2020

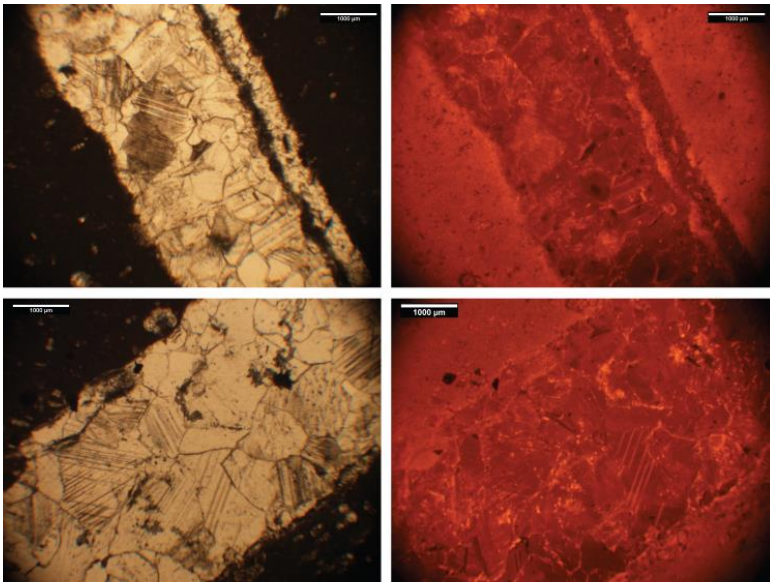

Figure 3: photomicrographs of various veins in natural light (left-hand side), with corresponding view under cathodoluminescence (right-hand side), top one is a set J1 vein from the Scaglia Fm., bottom one is a set J2 from the Maiolica Fm.

https://doi.org/10.5194/se-2020-64
Preprint. Discussion started: 5 May 2020

Solid Earth
Discussions

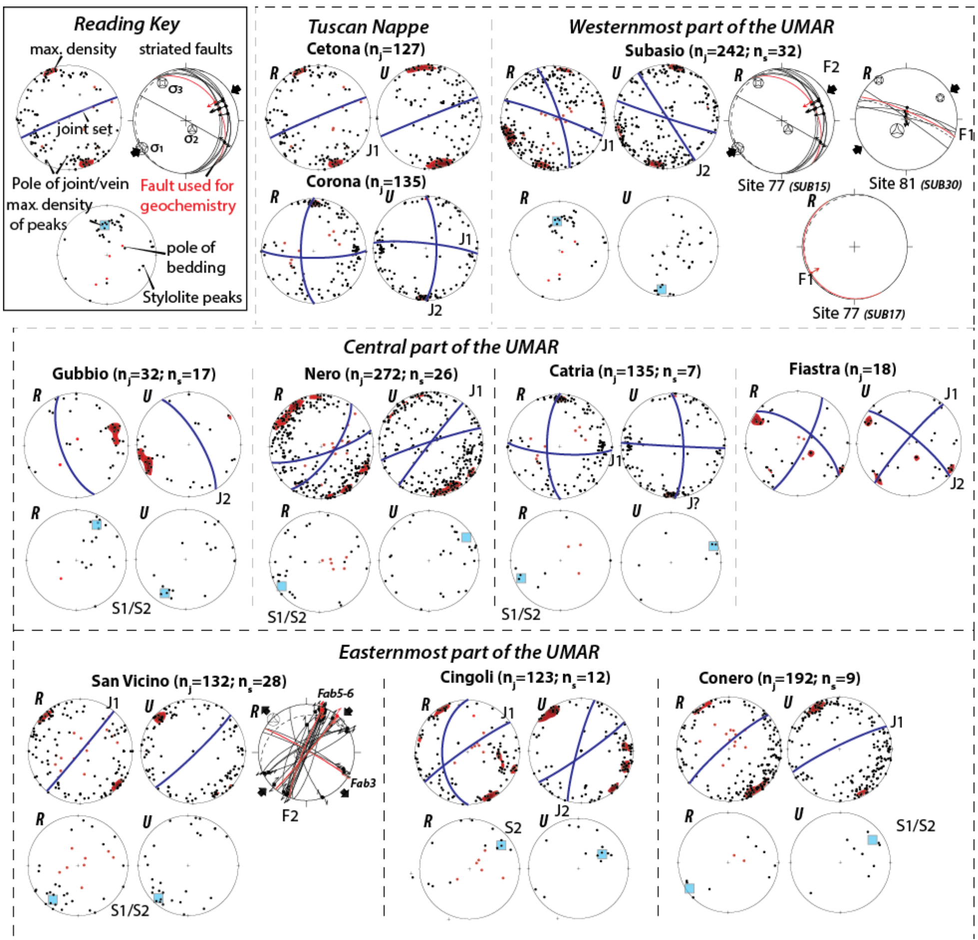

Figure 4: Poles of measured joints/veins and stylolite peaks projected on Schmidt stereograms, lower hemisphere, for the different structures. Data are projected in the current attitude of the strata (left, R), with pole to bedding in red, and after unfolding (right, U). Red color scale represents highest density according to Fischer statistical analysis using the software OpenStereo, and main fracture set average orientation are represented as blue planes. For tectonic stylolite peaks, the blue square represents highest density according to Fischer statistical analysis. Striated fault inversion results are reported in the current attitude of the strata (bedding as dashed line).

https://doi.org/10.5194/se-2020-64
Preprint. Discussion started: 5 May 2020

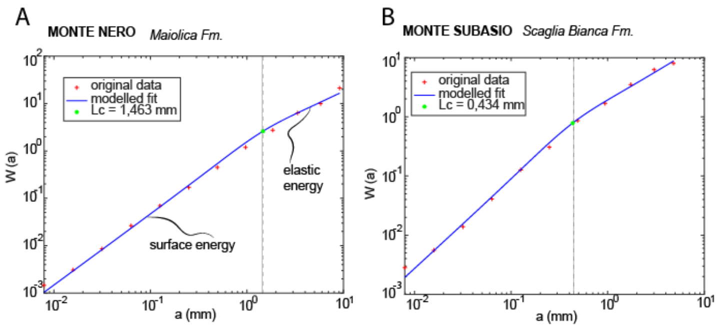

Figure 5: Examples of results of stylolite roughness inversion, with signal analysis by Average Wavelet in the Monte Nero (A) and in the Monte Subasio (B).

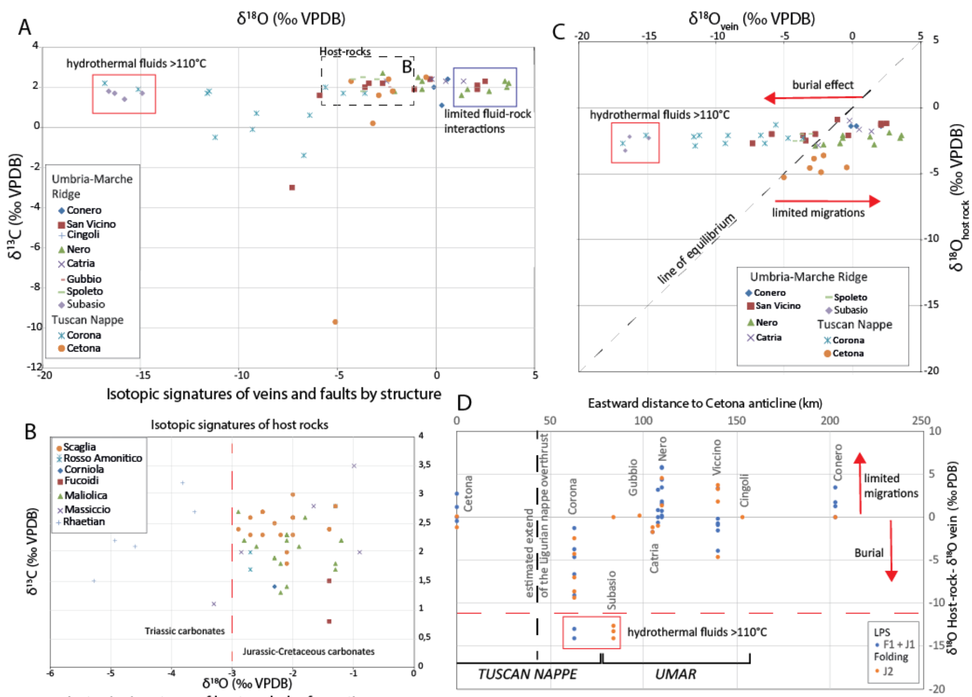

Figure 6: A) Plot of $\delta^{13}C$ vs $\delta^{18}O$ (‰ VPDB) of veins represented by structure. Frames represent the different type of fluid system. B) Plot of $\delta^{13}C$ vs $\delta^{18}O$ (‰ VPDB) of host-rocks represented by structure. C) Plot of δ^{18}Ovein vs δ^{18}Ohost (‰ VPDB) of veins represented by structures. D) Plot of the difference between δ^{18}Ohost-rocks and $\delta^{18}O$ veins (‰ VPDB) vs eastward distance from the Cetona Antincline towards the Adriatic basin across the strike of the UMAR. Data are represented by tectonic sets. The proposed extension of the Ligurian nappe overthrust is reported after Caricchi et al., 2014; red frames, arrows and lines represent the fluid systems.

https://doi.org/10.5194/se-2020-64
Preprint. Discussion started: 5 May 2020

Solid Earth
Discussions
Open Access

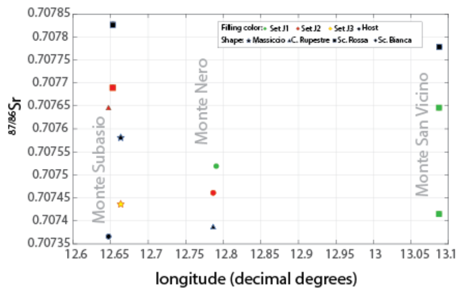

Figure 7: Plot of $^{87/86}Sr$ signatures vs longitude, with filling color related to tectonic set and point shape related to host rock formation.

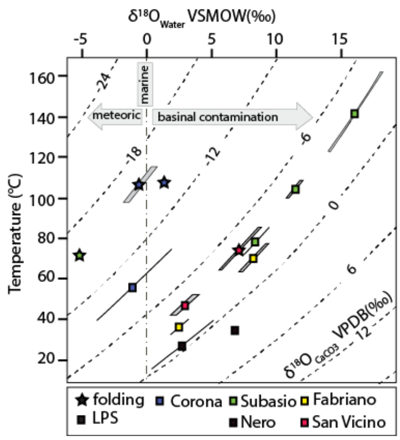

Figure 8: Plot of $\delta^{18}O_{fluid}$ (‰ SMOW) vs precipitation temperature (°C) obtained from clumped isotope analyses, oblique lines are the measured $\delta^{18}O_{CaCO3}$ of the vein cements (‰ PDB). Shape of the points correspond to tectonic set (LPS being U1 and compatible faults and folding U2), while filling color relates to structure. Oblique dotted lines are the measured $\delta^{18}O$ signatures of carbonates.

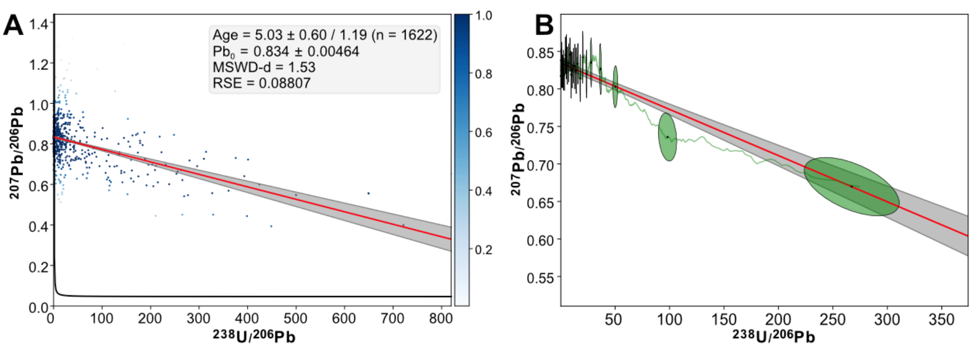

Fig. 9: A) Tera-Wasserburg concordia plot obtained from LA-ICPMS U-Pb dating of FAB5 calcite sample. The age was obtained by robust regression through the U-Pb image pixel values. The scale bar corresponds to the weight of each pixel as determined by robust regression. B) Same plot but with

https://doi.org/10.5194/se-2020-64
Preprint. Discussion started: 5 May 2020

discretized data represented as ellipses (one ellipse = 60 pixels). The running mean (window = 60 pixels) is also shown as green line.

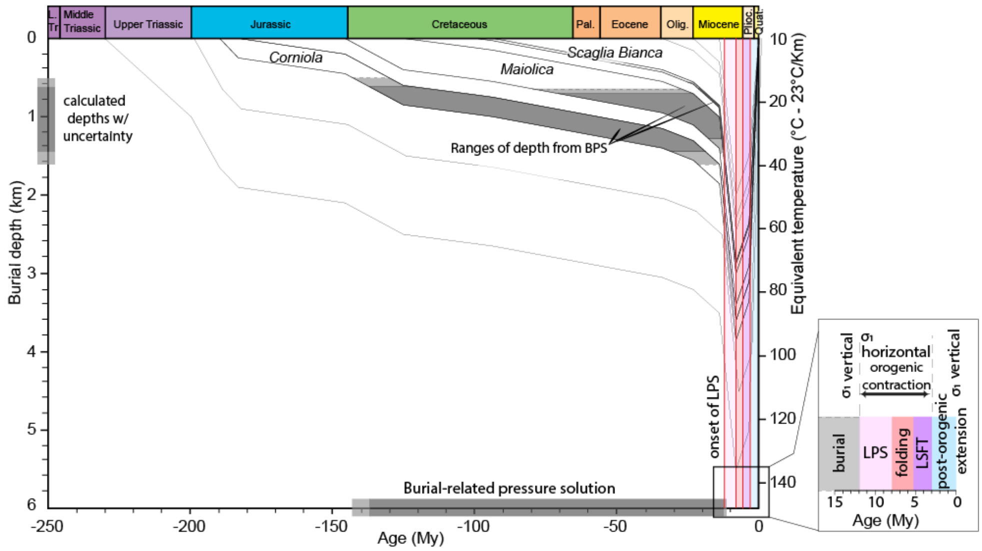

Figure 10: Burial model valid for the Umbria Marche Ridge, derived from well data and previously published burial models in the Tuscan Nappe (Caricchi et al., 2015). The range of depths reconstructed from bedding parallel stylolite roughness inversion (with uncertainty) are reported for each formation as grey shades. The derived corresponding timing and depth of active dissolution are reported on the x-axis and left y-axis, respectively. The timing of the deformation is reported on the right-hand side as a zoom. The onset of Layer Parallel shortening is deduced from the latest bedding stylolite to have been active, the onset of LSFT is given by U-Pb dating of fault coating in this study. The timing of folding and post-orogenic extension are reported from published sedimentary data (see text for more detailed explanations).

https://doi.org/10.5194/se-2020-64
Preprint. Discussion started: 5 May 2020

Solid Earth Discussions
Open Access
EGU

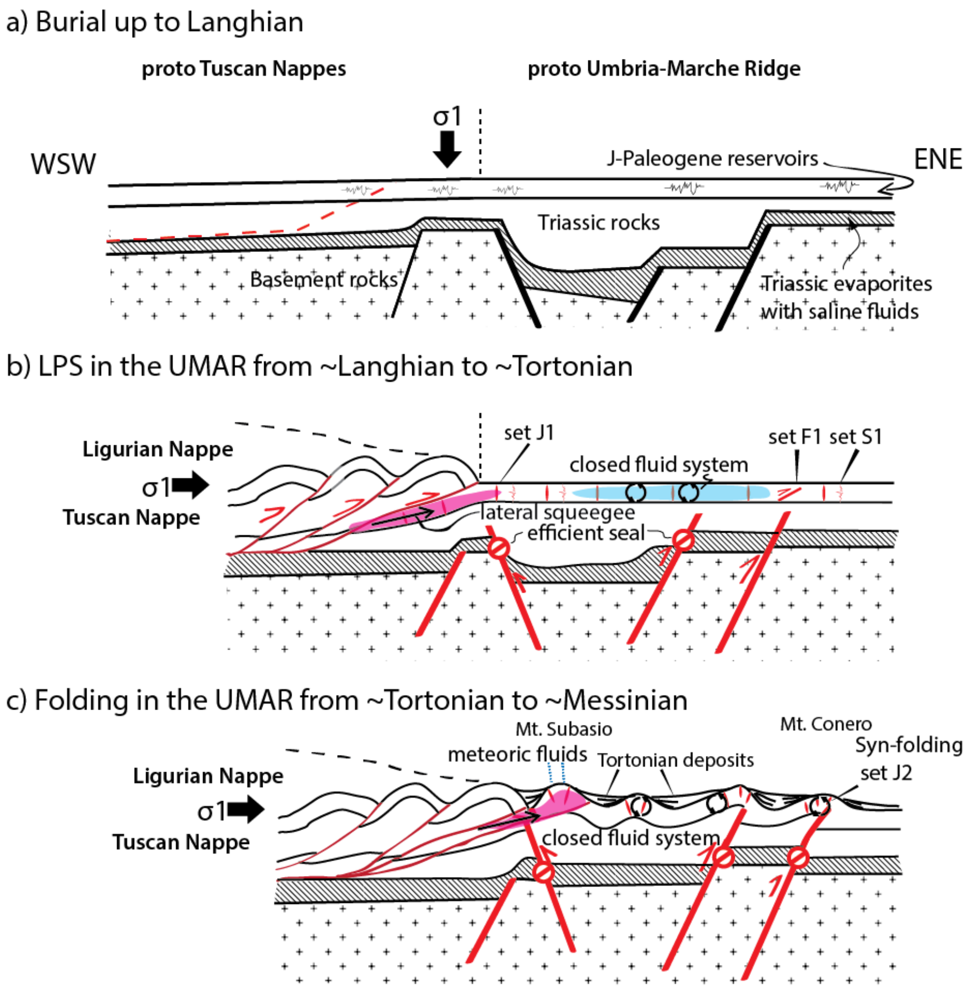

Figure 11: Conceptual model representing fracture development and regional scale fluid dynamics during the formation of the Tuscan Nappes and Umbria Marche Ridge. Red areas represent the extent of pulses of eastward hydrothermal fluids. Blue areas represent closed fluid system at the scale of the carbonate reservoirs.

https://doi.org/10.5194/se-2020-64
Preprint. Discussion started: 5 May 2020

Solid Earth Discussions
Open Access
EGU

Table 1 - Results of Stylolite Roughness Inversion applied on beddIng-parallel stylolites

Sample	GPS	location	formation	Lc (mm)*	E (GPa)	mu	v	vertstress (Pa)	depth (m)
	165	Subasio	Scaglia Bianca	1,059	23,2	0,25	0,32	21811000	926
	165	Subasio	Scaglia Bianca	1,306	23,2	0,25	0,32	19640000	834
	165	Subasio	Scaglia Bianca	0,46	23,2	0,25	0,32	33093000	1406
A165	165	Subasio	Scaglia Bianca	0,486	23,2	0,25	0,32	32196000	1368
	165	Subasio	Scaglia Bianca	0,434	23,2	0,25	0,32	34070000	1447
	165	Subasio	Scaglia Bianca	0,971	23,2	0,25	0,32	22778000	967
	165	Subasio	Scaglia Bianca	1,488	23,2	0,25	0,32	18400000	782
	110	Nero	Maiolica	1,073	23,2	0,25	0,32	21668000	920
	110	Nero	Maiolica	1,535	23,2	0,25	0,32	18116000	769
	110	Nero	Maiolica	1,463	23,2	0,25	0,32	18557000	788
	110	Nero	Maiolica	1,071	23,2	0,25	0,32	21688000	921
AN26	110	Nero	Maiolica	1,29	23,2	0,25	0,32	19762000	839
	110	Nero	Maiolica	1,073	23,2	0,25	0,32	22661000	962
	110	Nero	Maiolica	1,596	23,2	0,25	0,32	17767000	755
	110	Nero	Maiolica	0,659	23,2	0,25	0,32	27649000	1174
	110	Nero	Maiolica	0,696	23,2	0,25	0,32	26904000	1143
AN16	115	Nero	Maiolica	1,279	23,2	0,25	0,32	19847000	843
A137	148	Conero	Scaglia Bianca	2,073	23,2	0,25	0.32	15589000	662
A123-2	130	Gubbio	Corniola	0,428	23,2	0,25	0,32	34308000	1457
	130	Gubbio	Corniola	0,791	23,2	0,25	0,32	25237000	1072
A123	130	Gubbio	Corniola	2,35	23,2	0,25	0,32	14642000	622
	130	Gubbio	Corniola	1,457	23,2	0,25	0,32	18595000	790
A21	104	San Vincino	Maiolica	0,906	23,2	0,25	0,32	23581000	1002
	104	San Vincino	Maiolica	0,787	23,2	0,25	0,32	25414000	1079
	138	Spoleto	Scaglia Bianca	0,655	23,2	0,25	0,32	27733000	1178
	138	Spoleto	Scaglia Bianca	0,634	23,2	0,25	0,32	28189000	1197
A104	138	Spoleto	Scaglia Bianca	0,66	23,2	0,25	0,32	27628000	1174
	138	Spoleto	Scaglia Bianca	1,22	23,2	0,25	0,32	20321000	863
	138	Spoleto	Scaglia Bianca	0,749	23,2	0,25	0,32	25935000	1102
	138	Spoleto	Scaglia Bianca	1,322	23,2	0,25	0,32	19521000	829

* the crossover length is given within 12% uncertainty, using values for Young Modulus (E) of 23,2 Gpa (Beaudoin et al., 2014), Poisson ratio (mu) of 0,25 and an interfacial energy (v) of 0,32 $J.m^{-2}$

https://doi.org/10.5194/se-2020-64
Preprint. Discussion started: 5 May 2020

Solid Earth Discussions
Open Access
EGU

Table 2 - Results of stable isotopic signature of O, C, and radiogenic signatures of Strontium $^{86}Sr/^{87}Sr$

Sample	GPS	Formation	Structure	Set	$\delta^{18}O$ Vein ‰V-PDB	$\delta^{13}C$ Vein ‰V-PDB	$\delta^{18}O$ HR ‰V-PDB	$\delta^{13}C$ HR ‰ V-PDB	$^{87}Sr/^{86}Sr_{V}$	$^{87}Sr/^{86}Sr_{Hr}$
A94V	134	Retian *	Cetona	J1	-3,2	0,2	-3,2	-4,6		
A93V	134	Retian *	Cetona	J1	-2,9	1,6	-2,5	-3,82		
A95V	134	Retian *	Cetona	J1	-0,5	2,5	-3,2	-4,53		
A92V	134	Retian *	Cetona	J1	-4,3	2,3				
A89V	133	Retian *	Cetona	J1	-2,4	2,4	-3,6	-4,93		
A84V	133	Retian *	Cetona	J2	-2,2	1,8	-2,3	-3,62		
A86V	133	Retian *	Cetona	J2	-5,1	-9,7	-3,9	-5,28		
A76F	125	Maliolica	Corona	F1	-6,7	-1,4	-2,1	2,3		
A76V2	125	Maliolica	Corona	J1	-15,1	1,9	-2,1	2,3		
A76V1	125	Maliolica	Corona	J1	-11,2	-0,5	-2,1	2,3		
A72V	125	Maliolica	Corona	J2	-5,6	2	-1,3	1,8		
A76V3	125	Maliolica	Corona	J2	-9,1	0,7	-2,1	2,3		
A77V2	125	Maliolica	Corona	J2	-11,6	1,7	-2,2	1,8		
A77V1	125	Maliolica	Corona	J2	-11,5	1,8	-2,9	2,7		
A96V	135	Rosso Amonitico	Corona	J1	-16,8	2,2	-2,7	2		
A97bV1	135	Rosso Amonitico	Corona	J1	-6,4	0,6	-2,7	1,7		
A97bV2	135	Rosso Amonitico	Corona	J1	-9,3	-0,1	-2,7	1,7		
A98V1	136	Corniola	Corona	J1	-3,6	1,7	-2,3	1,4		
A98V2	136	Corniola	Corona	J2	-4,7	1,7	-2,3	1,4		
A121V	G	Maliolica	Gubbio	J2	-2,4	2	-2,6	2,1		
A112V1	141	Massiccio	Subasio	J2	-15,8	1,4				
A111V	141	Massiccio	Subasio	J2	-16,6	1,8	-3,3	1,1	0,707644	0,707366
A118V	145	Scaglio Rossa	Subasio	J2	-16,3	1,7	-2,2	2,3	0,707690	0,707827
A120V	145	Scaglia Rossa	Subasio	J2	-14,9	1,7	-2,3	2,5		
A116V	144	Massiccio	Subasio	J3					0,707437	0,707580
A59V	119	Maliolica	Catria	J1	1,4	2,3	-1,8	2,6		
A73V	122	Massiccio*	Catria	J1	-0,2	2,4	0,4	-0,99		
A63V	122	Massiccio*	Catria	J1	0,5	2,3	-0,3	-1,66		
A66V	122	Massiccio*	Catria	J2	-2,5	2,3	-1,5	-2,85		
A56V	118	Scaglia Cinera	Nero	J1	-0,9	2,5	-2,7	2,3		
A57bV	118	Scaglia Cinera	Nero	J1	-2,7	2,7	-2,9	2,4	0,707461	0,707382
A53V1	116	Maliolica	Nero	J1	-2,1	1,8	-2,8	2,2	0,707519	
A53V2	116	Maliolica	Nero	J1	1,6	1,9	-2,8	2,2		
A52V	115	Maliolica	Nero	J1	1,3	1,6	-2,2	1,3		
A50V1	113	Maliolica	Nero	J1	-0,7	2,3	-2,3	1,9		
A50V2	113	Maliolica	Nero	J1	3,5	2,3	-2,3	1,9		
A47V	112	Maliolica	Nero	J1	3,7	2,2				
A46V	112	Maliolica	Nero	J2	2,7	1,8	-1,9	2,1		
A44V	111	Maliolica	Nero	J1	3,6	2	-2,1	2,2		

https://doi.org/10.5194/se-2020-64
Preprint. Discussion started: 5 May 2020

A43V	110	Maliolica	Nero	J2	-0,7	1,9	-2,1	1,4		
A107F	139	Scaglia Rossa	Spoleto	F1	-4,2	2,4	-2,5	2,7		
A107V	139	Scaglia Rossa	Spoleto	J1	-3,7	2,5	-2,5	2,7		
A104V1	139	Scaglia Rossa	Spoleto	J2	-3,7	1,8	-2	2,6		
A27V	106	Massiccio	San Vicinno	J1	-1,1	1,9	-0,9	2		
A40F	109	Scaglia Bianca	San Vicinno	F1	-5,9	1,6	-2	3		
A38V	109	Scaglia Bianca	San Vicinno	J2	-7,3	-3	-2,7	2,6	0,707646	0,707778
A18V	104	Maliolica	San Vicinno	J1	2,1	1,9	-1,3	1,7		
A74V1	104	Maliolica	San Vicinno	J2	2,1	2,1	-1,2	2,2		
A74V2	104	Maliolica	San Vicinno	J2	2,5	2,3	-1,2	2,2		
A32V	108	Scaglia Bianca	San Vicinno	J1	-3,4	2,2	-2,5	2,3	0,707415	0,707778
A29V	108	Scaglia Bianca	San Vicinno	J1	-3,6	2	-2,1	1,8		
A34V	108	Scaglia Bianca	San Vicinno	J1	-2,7	2,2	-2	2,3		
A30V	108	Scaglia Bianca	San Vicinno	J2	-0,3	2,4	-2,1	2		
A14V	101	Scaglia	Cingoli	J2			-1,3	2,8		
A129bF	146	Scaglia	Conero	F1	2,1	2	-1,4	2,4		
A129bV	146	Scaglia	Conero	F1	-0,1	2	-1,4	2,4		
A126V	146	Scaglia	Conero	J2	0,6	2,4				
A133V	148	Fucoidi	Conero	J1			-1,4	1,5		
A135V	148	Fucoidi	Conero	J1	0,3	1,1	-1,4	0,8		

*: Values were corrected to reflect the fact that host rocks is dolomite; HR stands for Host Rock, V stands for Vein

https://doi.org/10.5194/se-2020-64
Preprint. Discussion started: 5 May 2020

Table 3 - Fluid precipitation temperature of oxygen isotopic signature derived from clumped isotope analysis

Sample Name	Structure	Set	Host formation	Mineralogy	Temperature (˚C)	MinT (˚C)	MaxT (˚C)	Fluid d18O VSMOW (mean)	Fluid d18O VSMOW (min)	Fluid d18O VSMOW (max)
A74A	Corona	J2	Maiolica	Calcite	106,4	98,0	115,4	-0,5	-1,8	0,9
A77-130	Corona	J2	Maiolica	Calcite	107,6	106,0	109,3	1,4	1,2	1,7
A77-40	Corona	J1	Maiolica	Calcite	55,9	39,9	74,7	-1,1	-3,9	1,9
A120	Subasio	J2	Scaglia Rossa	Calcite	71,7	71,7	71,7	-5,2	-5,2	-5,1
A28	Subasio	J1	Massiccio	Calcite	119,1	114,8	123,6	11,3	10,7	12,0
SUB15	Subasio	F1	Scaglia Cinerea	Calcite	78,3	71,7	85,3	8,4	7,4	9,5
SUB17	Subasio	F1	Scaglia Cinerea	Calcite	140,9	122,9	161,8	16,1	14,0	18,2
SUB30	Subasio	F1	Scaglia Cinerea	Calcite	104,4	100,1	108,9	11,4	10,8	12,1
A52	Nero	J1	Maiolica	Calcite	34,7	33,9	35,5	6,8	6,6	7,0
A56	Nero	J1	Scaglia Rossa	Calcite	27,2	15,9	39,9	2,7	0,3	5,2
A29	San Viccino	J1	Scaglia Rossa	Calcite	47,3	42,5	52,4	3,0	1,9	4,0
A39	San Viccino	J2	Scaglia Rossa	Calcite	74,5	64,7	85,2	7,2	5,6	8,8
FAB3	San Viccino	F2	Langhian Flysch	Calcite	36,5	32,8	40,3	2,5	1,7	3,3
FAB6	San Viccino	F2	Langhian Flysch	Calcite	70,3	63,7	77,4	8,3	7,1	9,4